Tectonophysics 801 (2021) 228719

Contents lists available at ScienceDirect

Tectonophysics

journal homepage: www.elsevier.com/locate/tecto

Enhancement of interplate coupling in adjacent segments after recent megathrust earthquakes

Mohammad Yuzariyadi *, Kosuke Heki

Dept. Natural History Sci, Hokkaido University, N10 W8, Kita-ku, Sapporo, Japan

ARTICLE INFO

Keywords:
Enhancement of Interplate Coupling
Megathrust earthquakes
GNSS
Subduction
Acceleration
Seismic cycle

ABSTRACT

Landward increase of surface velocity has been found for segments adjacent along-strike to megathrust faults after the 2003 Tokachi-oki and the 2011 Tohoku-oki earthquakes, NE Japan. A similar increase of landward velocities was reported for the segments to the north of the rupture of the 2010 Maule earthquake, Chile. We utilize available GNSS data to find such changes for six megathrust earthquakes in four subduction zones, including NE Japan, central and northern Chile, Sumatra, and Mexico to investigate their common features. Our study showed that such increase, ranging from a few mm/yr to ~1 cm/yr, appeared in adjacent segments following the 2014 Iquique (Chile), the 2007 Bengkulu (Sumatra), and the 2012 Oaxaca (Mexico) earthquakes in addition to the three cases. The region of the increased landward movements extends with spatial decay and reach the distance comparable to the along-strike fault length. On the other hand, the temporal decay of the increased velocity is not clear at present. The degree of increase seems to depend on the earthquake magnitude, and possibly scales with the average fault slip in the earthquake. This is consistent with the simple two-dimensional model proposed earlier to attribute the phenomenon to the enhanced coupling caused by accelerated subduction. However, these data are not strong enough to rule out other possibilities.

1. Introduction

Classical concept of the movement of forearc at convergent plate boundaries during a seismic cycle is the alternation of slow interseismic landward movement and sudden coseismic trenchward movement. The interseismic movements reflect interplate coupling that accumulates strain toward the next interplate earthquakes. Space geodetic observations since 1990s revealed the existence of a transient postseismic stage, i.e. forearcs move slowly trenchward during the early part of the seismic cycle (e.g. Wang et al., 2012). They are caused by postseismic processes such as afterslip (e.g. Heki et al., 1997) and viscous relaxation of asthenosphere (e.g. Ozawa et al., 2004). Recent advent of sea floor geodesy revealed postseismic landward motion of the oceanic lithosphere near the Japan Trench after the 2011 Tohoku-oki earthquake (M_w 9.0), which is considered a part of the viscous relaxation (Sun et al., 2014).

Heki and Mitsui (2013) reported unexpected increase of the landward movements of forearc GNSS stations in segments adjacent along-strike to the megathrust rupture after the 2003 Tokachi-oki earthquake (M_w 8.3), and possibly after the 2011 Tohoku-oki earthquake (Fig. 1). General features of this phenomenon are illustrated in Fig. 2. After earthquakes, GNSS stations near the ruptured fault would move trenchward (Fig. 2b). In addition to it, Heki and Mitsui (2013) found that stations on segments adjacent to the ruptured fault showed landward increase of movements as illustrated with green arrows in Fig. 2b. This looks as if interplate coupling in the neighboring segments of the rupture has increased.

This phenomenon cannot be explained by classical viscoelastic relaxation. Fig. 3 shows coseismic jump and slow movements caused by postseismic viscous relaxation calculated for a simple thrust earthquake case following Fukahata and Matsu'ura (2005, 2006). Postseismic deformation continues as the shear stress within viscous asthenosphere decays and let the deformation pattern reach the final state realizing the two-dimensional mechanical equilibrium within the lithosphere. Fig. 3b demonstrates that postseismic viscoelastic relaxation generates only trenchward movement of forearc GNSS stations. In other words, landward increase of velocity as seen for station X in Fig. 2 does not occur in the adjacent segments. This situation remains similar even with different settings of parameters, e.g. elastic thickness, viscosity of underlying asthenosphere, geometry of the fault. So, the postseismic acceleration of

* Corresponding author.
E-mail addresses: mohammad.yuzariyadi@gmail.com, myuzariyadi@eis.hokudai.ac.jp (M. Yuzariyadi), heki@sci.hokudai.ac.jp (K. Heki).

https://doi.org/10.1016/j.tecto.2021.228719
Received 3 June 2020; Received in revised form 25 December 2020; Accepted 27 December 2020
Available online 9 January 2021

landward velocities as shown in Fig. 2b would need an explanation with some other mechanisms.

Mavrommatis et al. (2014) suggested that the increased coupling in the northernmost Honshu after the 2003 Tokachi-oki earthquake (Segment 3 in Fig. 1b of Heki and Mitsui, 2013) reflects the termination of the afterslip of the 1994 M_w 7.6 Sanriku-oki earthquake (Heki et al., 1997). This, however, does not explain the landward velocity increase seen at the neighboring segment on the other side (Segment 1 in Fig. 1b of Heki and Mitsui, 2013) of the 2003 Tokachi-oki rupture. Small-scale change of interplate coupling can be explained by the pore fluid pressure changes associated with coseismic fluid migration along the plate interface (Materna et al., 2019). However, rapid fluid migration that enable coseismic enhancement of interplate coupling over hundreds of kilometers has never been found or predicted.

To explain the postseismic increase of landward velocity, Heki and Mitsui (2013) hypothesized that the coseismic stress drop modified the force balance acting on the slab around the ruptured segment and induced accelerated subduction of the oceanic plate (Anderson, 1975). As a seismological evidence, Uchida et al. (2016) found accelerated interplate creep rates from slip accumulation rates of small repeating earthquakes beneath the Kanto area following the 2011 Tohoku-oki earthquake. Outside NE Japan, Melnick et al. (2017) found the increased landward velocity also in Chile, at GNSS stations located to the north of the 2010 Maule earthquake (M_w 8.8) rupture. Melnick et al. (2017) called it super-interseismic period that occur at the early stage of an earthquake cycle, and Loveless (2017) considered it a common phenomenon after megathrust earthquakes.

Melnick et al. (2017) suggested that this enhanced landward velocity might have triggered the 2015 Illapel earthquake (M_w 8.3) and the 2016 Chiloé earthquake (M_w 7.6) that occurred to the north and south of the Maule rupture, respectively. Heki and Mitsui (2013) considered the accelerated subduction may account for temporary increase of regional seismicity such as the sequences of megathrust earthquakes in 1950s–1960s in Kamchatka-Aleutian subduction zones (Kanamori, 1978). Considering the large along-trench extent of these earthquakes, it would be difficult to explain such enhanced seismicity just as static stress perturbations (King et al., 1994).

The scope of the present study is to explore similar examples worldwide, taking advantage of the rapid expansion of GNSS networks in various subduction zones, using station coordinate data covering periods before and after megathrust earthquakes. We then try to find common features and discuss if the compiled data support a certain model, e.g. the slab acceleration model by Heki and Mitsui (2013).

2. Data and methods

2.1. GNSS data and station selection

We analyze GNSS data that are available in forearc regions of subduction zones such as the western Sumatra, the NE Japan, the central and northern Chile, and the Oaxaca region, Mexico (Fig. 1). In Japan, we use the daily coordinates of the F3 solutions of the GNSS Earth Observation Network (GEONET) stations provided by Geospatial Information Authority of Japan (Nakagawa et al., 2009). For the 2003 earthquake, we followed the procedure by Heki and Mitsui (2013) and fixed the Kamitsushima station, north of Kyushu, and compared the velocity difference before and after the earthquake. For the 2011 earthquake, the Kamitsushima station, ~1000 km away from the epicenter, exhibited a few mm/yr postseismic movements. Hence, we did not fix any stations and subtracted the movement of the landward plate calculated with the nnr-MORVEL56 plate motion model (Argus et al., 2011) from the coordinate changes in the F3 solution expressed in the International Terrestrial Reference Frame (ITRF).

In Sumatra, we analyzed the data from the Sumatran GPS Array (SuGAr) stations provided by Bandung Institute of Technology (Ardika et al., 2015). These data are processed using the GAMIT 10.5 to obtain

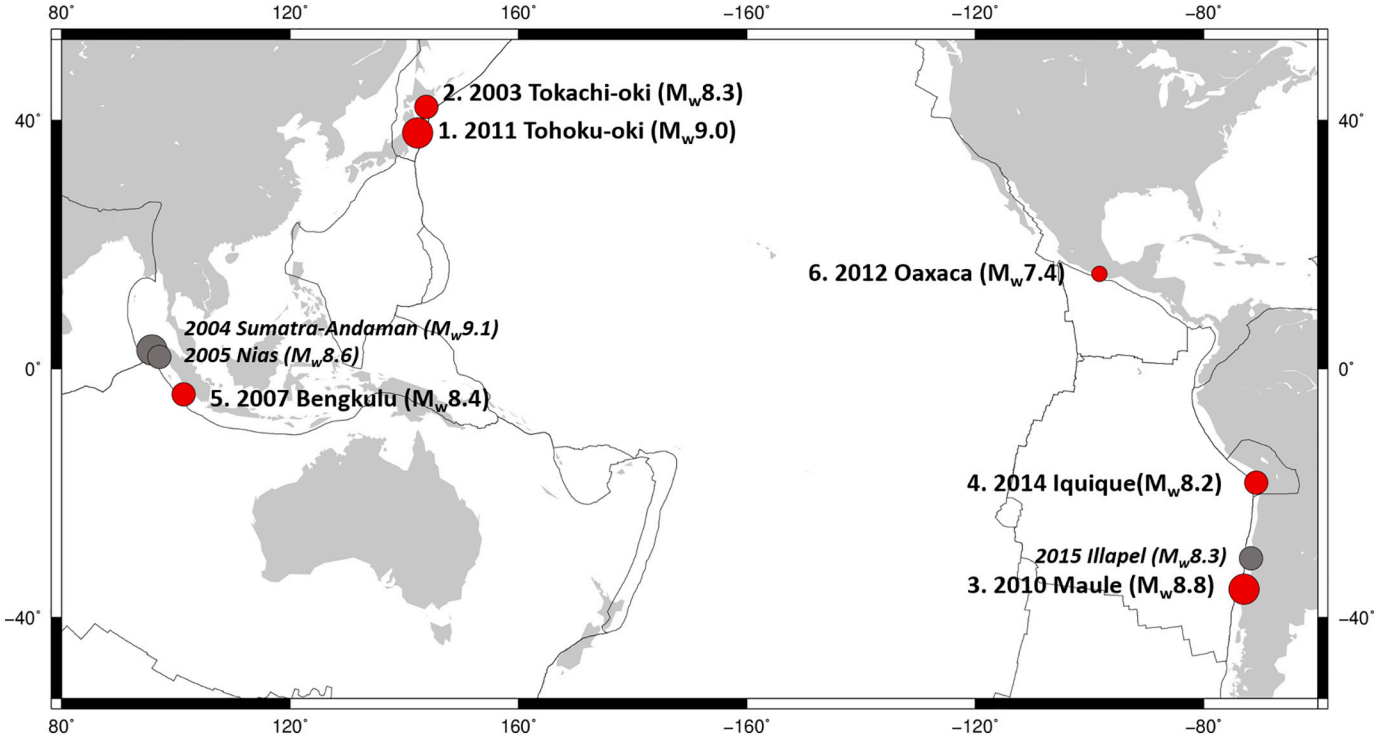

Fig. 1. Map of the locations of the earthquakes studied here. Red circles represent the six earthquakes that showed postseismic increased landward velocity in adjacent segments. Numbers attached to the earthquakes correspond to those in Table 1. Gray circles represent megathrust earthquakes that may have caused such velocity changes, but we failed to find enough GNSS data from stations in appropriate places with enough time span for pre- and postseismic periods (Section 5.1). (For interpretation of the references to colour in this figure legend, the reader is referred to the web version of this article.)

daily solutions (Herring et al., 2018). For the South and Middle American data, we analyzed the Precise Point Positioning (PPP) solutions available from the Nevada Geodetic Laboratory (Blewitt et al., 2018) and partly from Jet Propulsion Laboratory at sideshow.jpl.nasa.gov/post/series.html. These movements within ITRF were converted to those relative to the landward plate using the nnr-MORVEL56 model. Because we discuss the change in velocity before and after earthquakes, common bias to these velocities are cancelled, i.e. the present study is not so sensitive to the selection of the plate motion model.

Here we are interested in the change of crustal velocities in the forearc region of the segment adjacent along-trench to the megathrust ruptures (stations with green arrows in Fig. 2b). Therefore, we have to avoid GNSS stations suffering from postseismic trenchward movements (stations with black arrows in Fig. 2b). They are caused by afterslip and viscous relaxation of asthenosphere, and those for individual earthquakes are well documented in literatures such as Yamagiwa et al. (2014) for the 2011 Tohoku-oki earthquake, Miyazaki et al. (2004) for the 2003 Tokachi-oki earthquake, Klein et al. (2016) for the 2010 Maule earthquake, Hoffmann et al. (2018) for the 2014 Iquique earthquake, and Lubis et al. (2013) for the 2007 Bengkulu earthquake. To select stations showing landward velocity changes, we see not only the polarities of trench-normal velocities but also the distance of stations from the fault edge. This is because the phenomena we study tend to occur in a certain range of distance, i.e. they occur in forearc from the fault edge over a distance comparable to a half of the fault length. This will be discussed later in Section 5.3.

In calculating the velocity changes of the selected GNSS stations, we compare velocities during the two periods before and after the earthquakes (Table 1). These periods should be long enough to enable estimation of accurate velocities (longer than two years to robustly remove seasonal changes) and hopefully be immediately before and after earthquakes. Actually, we often have to shift or shorten these periods to avoid unwanted transient movements caused by other smaller earthquakes during the studied periods.

We should note that landward velocity changes depend on the selection of time windows. For example, such velocity changes are often unstable during the first few years while postseismic transient movements continue. We will discuss this problem comparing velocities in different time windows in Section 5.3.

We also need to pay attention to past earthquakes in nearby segments. Large interplate earthquakes are followed by trenchward postseismic movements of GNSS stations lasting for years. Their temporal decay might leak into the postseismic landward velocity increases, the target of the present study. For the six earthquakes studied here, we discuss potential influences from such past earthquakes.

2.2. Data related to earthquakes

In addition to the geodetic data, we downloaded data from US Geological Survey (earthquake.usgs.gov/earthquakes/map/) to draw slip distributions of the megathrust earthquakes. We also discuss changes in seismicity expecting positive correlation between relative plate velocities and seismicity (Ide, 2013). Here we try to detect increases in seismicity in the segment showing enhanced coupling after the 2011 Tohoku-oki and the 2010 Maule earthquakes. We downloaded data from the International Seismological Centre catalog (www.isc.ac.uk) with depth $\leq$ 60 km. We used the target events with magnitude body (m_b) in the period from 2000/01/01 to 2017/12/1 in the region 41.5° to 45°N, 143° to 149°E for the Tohoku-oki case, and from 2000/01/01 to 2017/12/1 in the region 33° to 27°S, 74° to 70°W for the Maule case.

Before comparing seismicity, it is important to check the magnitude completeness (Mc) of the earthquake catalog. By applying the method by Wiemer and Wyss (2000), we plot the cumulative number of earthquakes versus magnitude to evaluate Mc. For the ISC catalog, we found Mc are 3.8 and 4.2 for the Tohoku-Oki and the Maule earthquakes, respectively. Then, we counted 1813 and 2066 earthquakes with Mb $\geq$3.8, and $\geq$ 4.2 for de-clustering process of the two earthquakes.

To compare seismicity changes by large earthquakes, it is also necessary to remove clustered earthquakes such as swarms and aftershocks from the catalog, e.g. by using a stochastic de-clustering method developed by Zhuang et al. (2004). This method discriminates seismicity into background and triggered events based on an epidemic-type aftershock sequence (ETAS) model. Parameters estimated by fitting the ETAS models to the ISC catalog are listed in Table A1. After de-clustering process, 1331 and 761 events remained as background events for the 2011 Tohoku-oki and the 2010 Maule cases. We discuss changes in these background events later in Sections 4.1 and 4.3.

2.3. A diagram indicating the postseismic enhanced coupling

In Section 4, we show a set of figures as shown in Fig. 4, for each megathrust earthquake. We model the time series of the two horizontal components of a GNSS station coordinate considering linear trends, average seasonal (annual and semiannual) changes, jumps associated with antenna replacements (for GEONET stations), and coseismic jumps. In addition to these standard parameters, we estimate the coseismic changes in velocity (v'-v). The velocities are expressed relative to the stable part of the landward plates of the subduction zones (Fig. A1). We also discuss possible existence of non-linear movements shortly after earthquakes and their influences in Section 5.3.

We first rotate the two horizontal axes (north and east) so that the

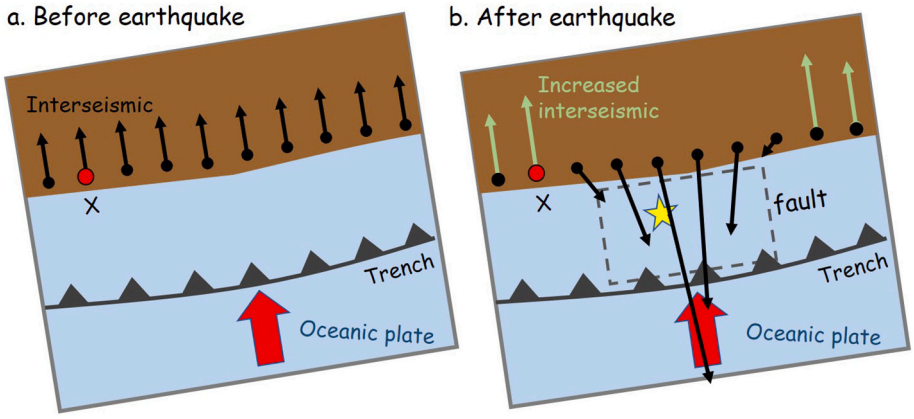

Fig. 2. Schematic illustration of interseismic movements of GNSS stations (a) and their changes by a large earthquake (b). The trenchward movements in (b) occur driven by afterslip and postseismic relaxation around the ruptured fault. In addition to this, interseismic landward velocities often increase in segments adjacent along-trench to the ruptured segment (station X).

two components coincide with the direction parallel with (red in Fig. 4a) or perpendicular to (blue in Fig. 4a) the interseismic movement of the station before the earthquakes (normally in the direction of the subducting oceanic plate). In the plot, we subtract the estimated average seasonal components. In the diagram, the coseismic increase of the landward velocity of a GNSS station appears as the positive change in the slope of the red time series (Fig. 4a). The blue (trench-parallel) component represents the change in the direction of the movement by the earthquakes. This is expected to be small. Both components often show coseismic jumps, but they are not the target of the present study.

Here, we do not discuss vertical components because changes in vertical velocities are not significant as reported for the 2003 case in Heki and Mitsui (2013). This partly comes from intrinsic large uncertainty in determining the vertical positions. Fig. A2 shows that vertical velocities changes following the 2011 Tohoku-oki earthquake are insignificant and non-systematic in direction. The figure also shows the vertical coordinate time series of two Chilean stations before and after the 2010 Maule earthquake. They suggest it difficult to extract meaningful changes in vertical velocities by this earthquake.

To see the whole picture of the postseismic increase of interplate coupling, we need lots of stations deployed at various distances from the megathrust fault. Typically, postseismic trenchward velocities dominate near the fault. Then, landward increased velocities (enhanced coupling signature) emerge as we go away along trench from the fault (Fig. 2b). This enhanced coupling would then decay as we go farther away from the fault.

It is usually difficult to see them all due to the insufficient availability of GNSS stations along the forearc. In this study, we use multiple stations to represent the landward velocity change whenever possible. Nevertheless, we sometimes have to let just one station represent the increase of the landward velocity for certain earthquakes. In the discussion, we compile all the cases to extract common features so that we can discuss the physical model behind the phenomenon.

For very large earthquakes, postseismic velocity changes can occur in a continental scale as shown in Melnick et al. (2017) in South America following the 2010 Maule earthquake and in China following the 2011 Tohoku-oki earthquake (Shao et al., 2015). In this study, we focus on the velocity changes occurring near the ruptured faults.

Table 1
Two periods used to estimate velocity changes before and after the earthquakes (Fig. 1).

No.	Earthquake (M_w)	Before earthquake	After earthquake[c]
1	2011/3/11 Tohoku-oki (9.0)	2008.00–2011.19	2011.19–2015.00
2	2003/9/25 Tokachi-oki (8.3)	1996.00–2003.74[a]	2003.74–2010.10
3	2010/2/28 Maule (8.8)	~2008.00[b]–2010.16	2010.16–2014.70
4	2014/4/1 Iquique (8.2)	~2010.00[b]–2014.25	2014.25–2019.25
5	2007/9/12 Bengkulu (8.4)	2005.50–2007.70	2007.70–2010.81[d]
6	2012/3/20 Oaxaca (7.4)	2010.38–2012.22	2012.22–2017.22

[a] Shifted to 1996.0–2003.0 to avoid influence of the Miyagi-oki earthquake (M_w 7.0) on 2003 May 26 for stations close to its epicenter
[b] Earliest possible starting times are used depending on the availability of the stations
[c] The early non-linear postseismic periods avoided to draw Figs. 6a, 7a, and 8a.
[d] Only data until the occurrence of the 2010 Mentawai earthquake are used.

3. Slab acceleration model by Heki and Mitsui (2013)

The purpose of this paper is to collect as much geodetic information as possible to facilitate the discussion on the model responsible for the postseismic landward change in velocities. We do not aim at proving a particular model, including the model by Heki and Mitsui (2013). In fact, there are attempts to explain postseismic landward velocity changes within the framework of viscous relaxation. For example, Melnick et al. (2017) reports results by a three-dimensional thermo-mechanical model to reproduce continental scale postseismic velocity changes. D'Acquisto et al. (2020) try to explain the observed changes as the elastic bending in a horizontal plane in response to the postseismic trenchward movement near the rupture area. Other models capable of explaining the observations may also emerge in future. Here, as one of the possibilities, we review the simple slab acceleration model Heki and Mitsui (2013) proposed to explain the landward increased movements in segments adjacent along-strike to a megathrust rupture.

Fig. 5a indicates the balance of forces acting on a subducting slab during an interseismic period. There, two down-dip forces, slab pull *Fsp* and ridge push *Frp*, are balanced with the two up-dip forces, side (partially bottom) resistance *Fsr* exerted by the surrounding asthenosphere and interplate coupling *Fc* at the plate interface. *Fsr* is

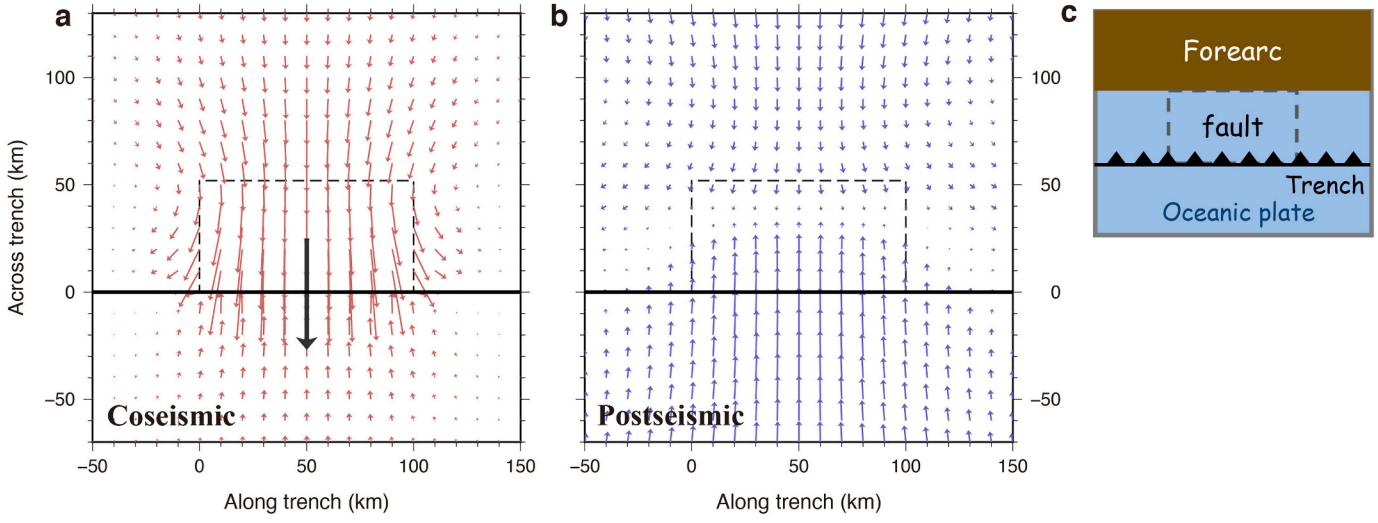

Fig. 3. Coseismic (a) and postseismic (b) surface displacement by reverse faulting occurring at a fault (dashed rectangle) dipping from the trench (solid line) in a tectonic setting shown in (c), calculated using the software package by Fukahata and Matsu'ura (2005, 2006). We assume a fault 100 × 60 km, with the dip angle 30° and the depth range 0–30 km. We assume lower viscoelastic layer (viscosity 10^{19} Pa s) beneath the upper elastic layer (thickness 30 km). A thick black arrow in (a) is the surface projection of the coseismic slip vector. (b) indicates the postseismic displacement caused by viscous relaxation of the lower layer after a period 10,000 times as long as the Maxwell time. Here, we can see that the viscoelastic relaxation generates trenchward and landward movements of grid points on land and sea, respectively, but does not make the pattern like Fig. 2b. The purpose of this figure is just to show patterns of displacements, and scales are not given for the arrows.

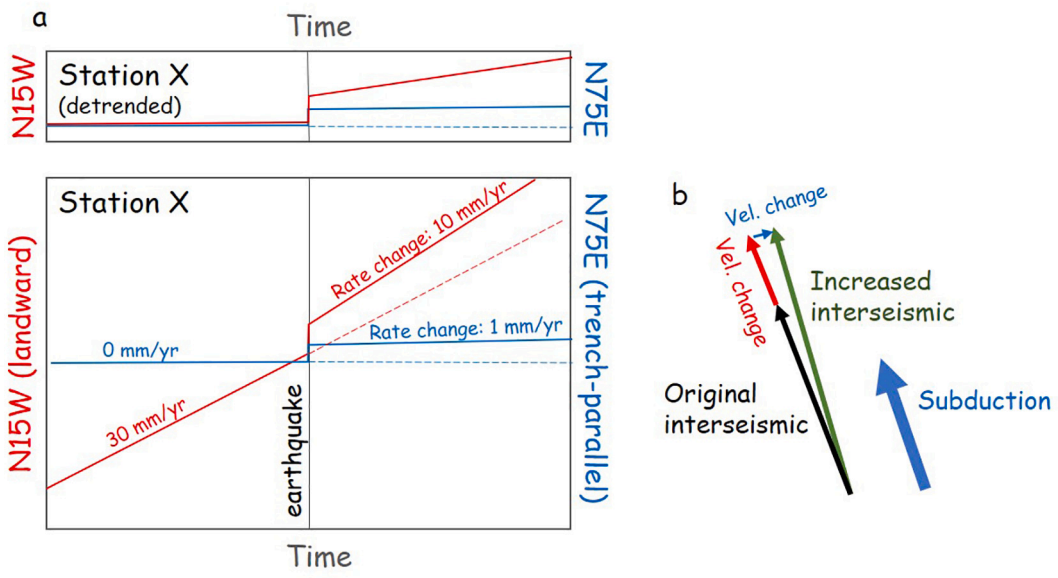

Fig. 4. An example of the analysis of the velocity change after a large earthquake for the station X shown in Fig. 2. (a) We rotate the horizontal axes so that one axis coincides with the interseismic movement direction (red) and the other axis is perpendicular to it (blue). Thus, the increase of the landward velocity of a GNSS station can be seen as the increased slope of the red component. In the small panel atop, we remove the pre-earthquake linear trend (dotted line) to isolate postseismic changes in trend. Y-axis represents the movement in the trench-normal (landward) and tranch-parallel azimuths. (b) Concept of the increased interseismic velocity which is the sum of the interseismic velocity before the earthquake and the coseismic velocity change. (For interpretation of the references to colour in this figure legend, the reader is referred to the web version of this article.)

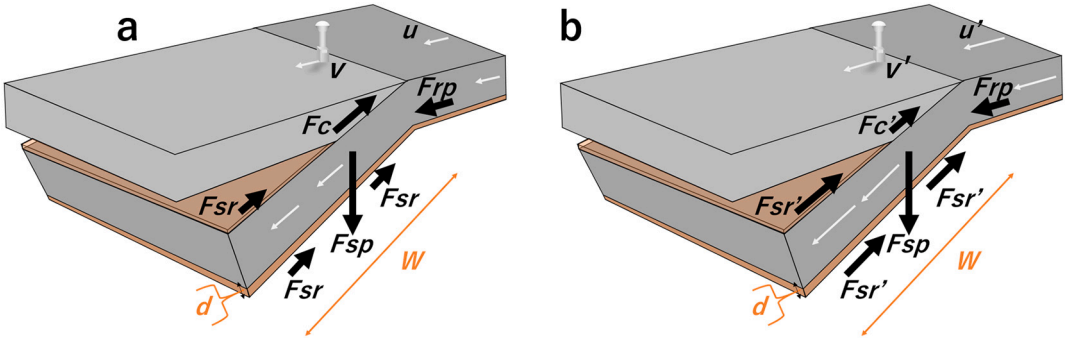

Fig. 5. Schematic view of the slab acceleration model, redrawn after Heki and Mitsui (2013). (a) and (b) show forces acting on a subducting slab before and after a megathrust earthquake, respectively, with a large stress drop. In (a), downward forces (*Fsp*: slab pull, *Frp*: ridge push) are balanced by upward forces (*Fc*: interplate coupling, *Fsr*: side resistance). In (b), sudden decrease of the coupling *Fc* to *Fc'* is compensated by the increase of *Fsr* to *Fsr'* realized by the slab acceleration from *u* to *u'*. The velocity of GNSS station before and after the earthquake is indicated by *v* and *v'*. *W* is the total trench-normal length of slab surface (both upper and lower surfaces) where viscous braking works, and *d* is the thickness of the thin low viscosity layer at the lithosphere-asthenosphere boundary.

proportional to the subduction speed u and we assume the resistance occurs in a thin low-viscosity layer at the slab surface. This is a two-dimensional model and the forces represent those working on a thin slice with a unit thickness.

Occurrence of a megathrust earthquake would reduce the coupling from *Fc* to *Fc*', which would be compensated by the increase of the side resistance caused by the acceleration of the subduction speed from u to u'. Let *Fc-Fc'* be the lost coupling (stress drop integrated along-dip), and it can be related to the slab acceleration u'-u as follows.

$$Fc - Fc' = Fsr' - Fsr = (u' - u)\,\mu W/d \tag{1}$$

where μ is the viscosity of the low-viscosity layer with the thickness of d, and W is the along-dip slab length (both upper and lower surface) where viscous braking works. Then, the acceleration u'-u is expressed as.

$$u' - u = (Fc - Fc')\,d/\mu W \tag{2}$$

For the same subduction zone with uniform μ, W and d, the acceleration u'-u would be proportional to *Fc-Fc*'. Larger earthquakes would accelerate the slab more strongly with a larger *Fc-Fc'*. It is actually the product of the fault width (along-dip length) D and the stress drop $\Delta\sigma$.

$$Fc–Fc' = \Delta\sigma\, D \tag{3}$$

Using the average slip s_{av}, $\Delta\sigma$ can be expressed using the rigidity ν as.

$$\Delta\sigma = \nu\, s_{av}/D \tag{4}$$

For the same subduction zone, we assume ν is the same. Then eqs. (3) and (4) suggest that *Fc-Fc*', and hence $u' - u$, scales with the average slip s_{av}, i.e.,

$$u'–u = (d\nu/\mu W)\, s_{av} \tag{5a}$$

In the present paper, we compare cases in different subduction zones. It is generally difficult to infer diversity of parameters ν, d, and μ for different subduction zones. However, we can know W from seismological studies. In other words, by assuming that $\nu\, d/\mu$ is the same, we could

examine if the observed slab acceleration u'-u is proportional to s_{av}/W,

$$u'-u = (\nu d/\mu)\, s_{av}/W \quad (5b)$$

In Section 5.6, we examine if the observed velocity changes for different megathrust earthquakes in various subduction zones obey eqs. (5a) and (5b).

4. Enhanced interplate coupling after various megathrust earthquakes

4.1. The 2011 Tohoku-oki earthquake (M_w 9.0)

The 2011 March Tohoku-oki earthquake occurred as the result of subduction of the Pacific plate beneath NE Japan arc on the Okhotsk (or North American) plate at the Japan Trench. Its source region included areas with a range of M7 to M8 earthquakes during the last few hundreds of years prior to the 2011 Tohoku-oki earthquake (Tajima et al., 2013), and geodetic data both on land and seafloor revealed the extremely large slip extending to the shallow portion of the plate boundary (e.g. Iinuma et al., 2012). The large-scale postseismic deformation of this earthquake due to afterslip and viscoelastic relaxation followed the earthquake (e.g. Yamagiwa et al., 2015), and east-southeastward velocity of coastal stations of the Tohoku District, NE Japan, still continues in 2020 (mekira.gsi.go.jp). Heki and Mitsui (2013) found that the interplate coupling has increased following this earthquake in eastern Hokkaido, the segment to the northeast of the Tohoku-oki rupture.

Fig. 6a shows the difference of the velocities before and after the 2011 Tohoku-oki earthquake. There, the start time of the period to estimate postseismic velocity is shifted to 2012.0 to avoid the strong non-linear behavior of the early part of the postseismic time series. The movements of the stations are reasonably linear in this period, but possible influences of non-linear movements are discussed later in Section 5.4. We can see that trenchward postseismic movements prevail in the Tohoku District and the western half of Hokkaido. The eastern Hokkaido shows, on the other hand, the typical enhanced interplate coupling signature, i.e. the velocity changes are northwestward. In drawing velocities in Fig. 6, we converted the velocity in ITRF to the frame fixed to the Okhotsk plate using the nnr-MORVEL56 model (Argus et al., 2011).

Fig. 6b, c shows crustal movements before and after the 2011 Tohoku-oki earthquake at ten stations 0519, 0512, 0009, 0125, 0531, 0010, 0112, 0138, 0015, and 0532 (from northeast to southwest). Because the postseismic trenchward movements of the 2003 Tokachi-oki earthquake still continued in 2011, their velocity vectors deviate significantly in azimuth from the subduction direction of the Pacific Plate. Nevertheless, as seen in Fig. 6a, the velocity changes at 2011.19 is clearly in the direction of the subduction, i.e. the pre-earthquake landward movement of the GNSS stations has increased after the 2011 Tohoku-oki earthquake.

In Fig. 6d, we show the diagram similar to Fig. 4 for the station 0112, where the landward velocity increase of 8.8 ± 0.1 mm/yr is seen. Such an error for the increase represents 2σ. It is scaled with post-fit residuals but may underestimate the real uncertainty. For the cases with data available from multiple stations, we use the scatters of their increase to express their uncertainties for later discussions of the model. One large difference from the typical case (Fig. 4) is that even the component perpendicular to the subduction direction (trench-parallel, blue component in Fig. 6d) has significant slopes. This component simply reflects the continuation of the postseismic movement of the 2003 Tokachi-oki earthquake, and these slopes do not show any change by the 2011 Tohoku-oki earthquake. Similar time series from two additional stations are given in Fig. A3. Change in seismicity in the region showing enhanced landward movements are discussed in Section 5.2. We also demonstrate that the postseismic movements of the 2003 Tokachi-oki earthquake are linear enough in 2008–2011 and its curvature does not influence the postseismic velocity change of the 2011 earthquake in Section 5.4.

4.2. The 2003 Tokachi-oki Earthquake (M_w 8.3)

The 2003 September Tokachi-oki Earthquake occurred at the Kuril Trench off the eastern Hokkaido as a possible recurrence of the 1952 M_w 8.2 Tokachi-oki earthquake. Postseismic deformation signatures observed using the GEONET data are well documented (e.g. Miyazaki et al., 2004; Itoh and Nishimura, 2016). Heki and Mitsui (2013) found postseismic enhanced interplate coupling, for the first time, at the segments adjacent northeastward and southwestward to the ruptured segment after this earthquake.

Fig. 7 shows the maps and diagram similar to Fig. 6 for the 2003 Tokachi-oki earthquake. We selected the GNSS stations with landward velocity changes located along the Pacific coast of the northernmost Honshu (stations with green vectors in Fig. 7a, 0153, 0156, 0158, 0162, 0027, 0539 from north to south). Fig. 7a, b shows interseismic velocities before and after the earthquake. Here we used the F3 solution and followed the procedures in Heki and Mitsui (2013), i.e., we fixed the Kamitsushima station, Kyushu, Japan, which is not much different from the frame fixed to the Okhotsk plate used for the 2011 earthquake (Fig. 6). In Fig. 7d, we show time series of the trench-normal (red) and trench-parallel (blue) components for the 0027 station. There we can see the increased landward movement of 5.3 mm/yr. Similar time series from two additional stations are given in Fig. A4.

As reported in Heki and Mitsui (2013), we also found that the velocity in the trench-parallel direction (N9.0E) has also changed the rate by −4.0 ± 0.1 mm/yr. This reflects the slight counterclockwise rotation of the velocity as recognized by comparing Fig. 7b and c. This might be due to postseismic viscous relaxation occurring as a slow movement away from the fault (together with the trenchward movement), which is visible in the numerical simulation results given in Fig. 3b. Similar outward movements are also reproduced by vertical axis crustal rotation in Melnick et al. (2017).

As described earlier, Mavromatis et al. (2014) suggested that this landward velocity change indicates the termination of the postseismic trenchward movement caused by the 1994 M_w7.6 Sanriku-oki earthquake (Heki et al., 1997). We do not think it a significant factor partly because their model does not explain the landward velocity change on the other side (easternmost Hokkaido) after the 2003 earthquake (Fig. 7a). In addition to that, we analyzed the velocity of 0027 prior to the 2003 earthquake. As shown in Fig. A7, the effect of postseismic transient of the 1994 Sanriku-oki earthquake remains dominant only until 1997–1998. We excluded data before 1998.0 in deriving the pre-2003 velocity (Fig. 7d), so that the postseismic transient of the 1994 earthquake do not affect the estimated velocity increases.

4.3. The 2010 Maule Earthquake (M_w 8.8)

Fast convergence between the Nazca and the South American plates causes recurrent megathrust earthquakes along the Peru-Chile Trench off the Pacific coast of South America. The 2010 February Maule earthquake, one such event in central Chile, filled the seismic gap lasting since the 1835 Conception earthquake. In addition to the co- and postseismic crustal deformation of this earthquake reported in Vigny et al. (2011), Moreno et al. (2012), and Klein et al. (2016). Melnick et al. (2017) reported postseismic increase of the landward velocities of stations located to the north of the rupture. They suggested that such enhanced coupling may have triggered the occurrence of the 2015 Illapel earthquake (M_w 8.3) to the north of the 2010 rupture.

Klein et al. (2016) reported large-scale postseismic oceanward movements of GNSS stations around the ruptured segment, and it can be seen in velocity changes by the 2010 earthquake in Fig. 8a. We also can see that stations located to the north of the 2010 rupture show clear signatures of enhanced interplate coupling (green vectors in Fig. 8a). The velocities of these GNSS stations before and after the earthquake are

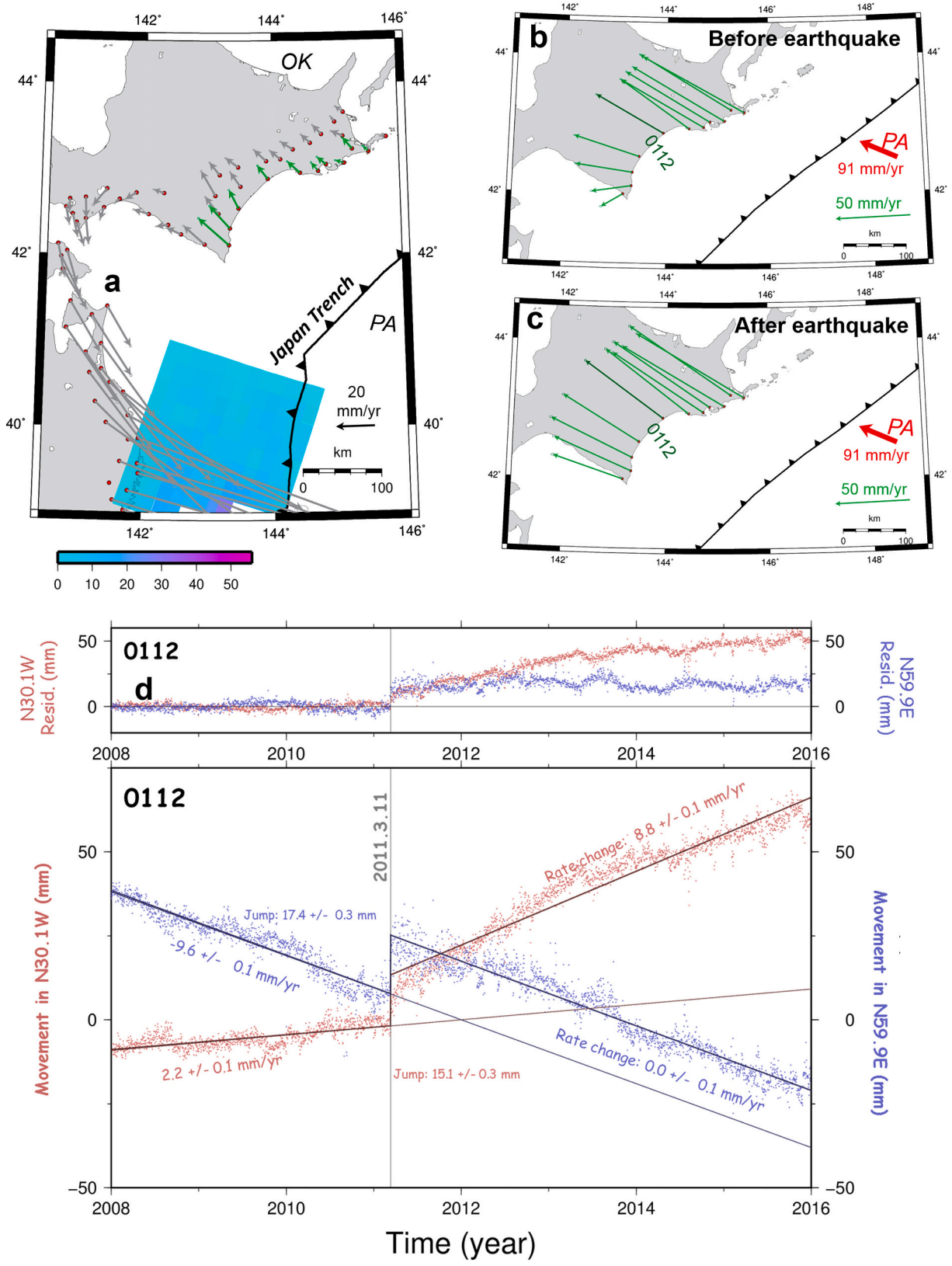

Fig. 6. (a) Differences of the velocities following the 2011 Tohoku-oki earthquake (during 2012.00–2015.00) relative to the reference velocities before the earthquake. GNSS stations with green arrows in (a) are free from the trenchward postseismic crustal movement, caused by afterslip and viscoelastic relaxation, and are used for further analyses. In (b) and (c), the green arrows show interseismic landward movements of GNSS stations before and after the 2011 Tohoku-oki earthquake relative to the Okhotsk plate (Table 1 summarizes the periods used to estimate these velocities). The red arrow represents the Pacific plate movement relative to the Okhotsk plate (Argus et al., 2011). Error ellipses show 2σ errors. (d) shows the time series of the 0112 station, the dark green arrow in (b), (c). See Fig. 4 for the meaning of red (trench-normal, N43.9 W here) and blue (trench-parallel, N46.1E here) components. The top panel of (d) shows the de-trended time series. (For interpretation of the references to colour in this figure legend, the reader is referred to the web version of this article.)

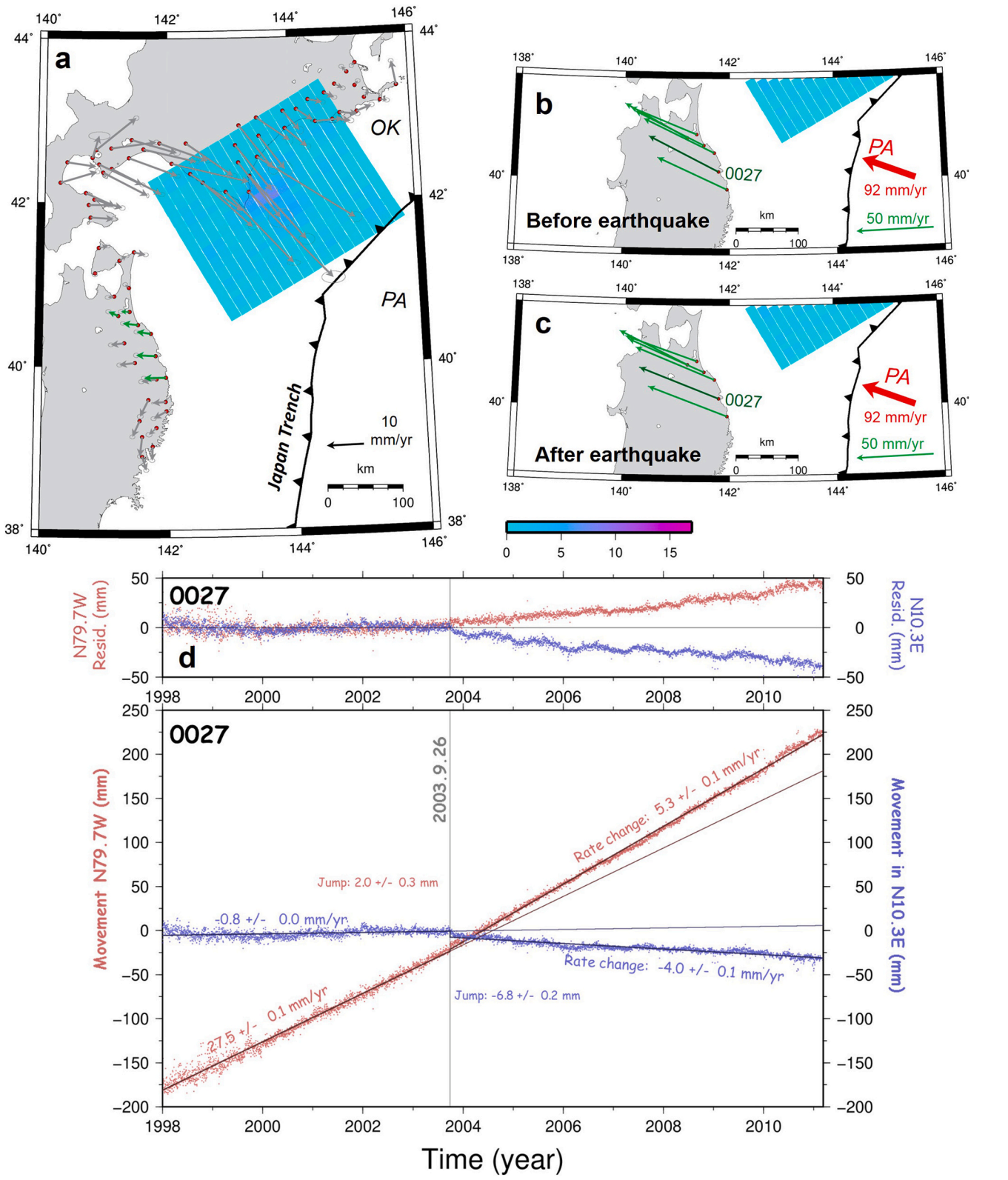

Fig. 7. Maps and diagram demonstrating the postseismic landward velocity changes for the 2003 Tokachi-oki earthquake. Meaning of symbols are the same as those in Fig. 6. (a) Differences of the velocities in 2008.7–2010.0 relative to the pre-2003.00 velocities (we removed data before 1998.0 to avoid influences from post-seismic movements of the 1994 Sanriku earthquake, see Section 5.4), reproduction of a part of Fig. 2a of Heki and Mitsui (2013). In (b) and (c), we compare the velocities before and after the 2003 earthquake for stations showing postseismic enhanced coupling in (a). Red arrow represents the Pacific plate movement relative to the Okhotsk plate (Argus et al., 2011). The time series of the 0027 station (dark green arrow in b, c) is shown in (d) for the trench-normal (red) or trench-parallel (blue) components. (For interpretation of the references to colour in this figure legend, the reader is referred to the web version of this article.)

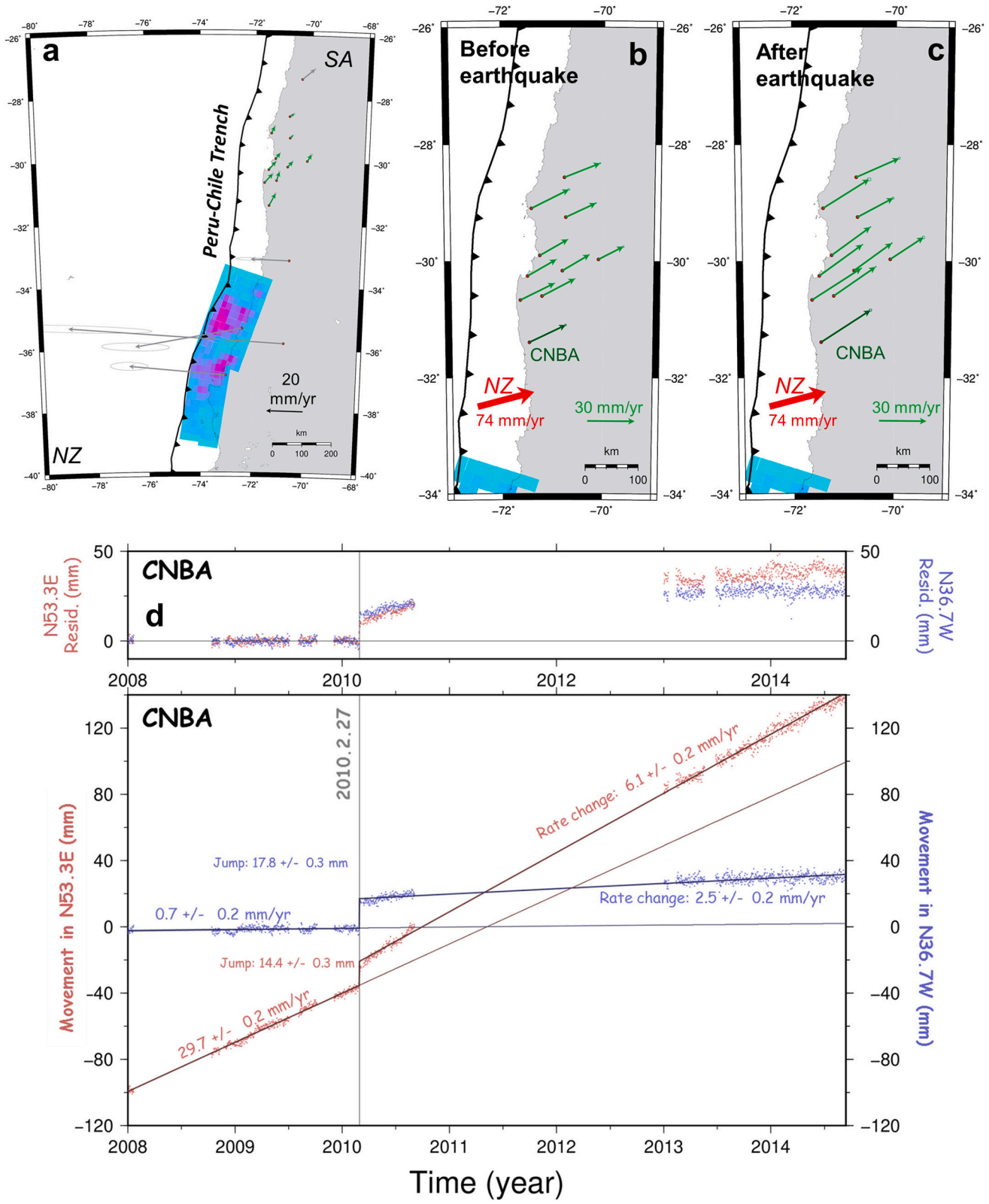

Fig. 8. Maps and diagram demonstrating the postseismic landward velocity change for the 2010 Maule earthquake. (a) Differences of the postseismic velocities from those before the earthquake. In (b) and (c), we compare the velocities before and after the earthquake for stations showing enhanced coupling. The red arrow represents the Nazca plate velocity. These velocities are all relative to the South American plate. The time series of the CNBA station (dark green arrow in b, c) is shown in (d) using the horizontal directions parallel with (red) or perpendicular to (blue) the velocity before the earthquake. If we exclude data from 2010.17–2011.00, the rate change is reduced to 5.0 ± 0.2 mm/yr. (For interpretation of the references to colour in this figure legend, the reader is referred to the web version of this article.)

shown in Fig. 8b and c, respectively. Fig. 8d shows the horizontal movement in the direction parallel with (red) and perpendicular to (blue) the before-earthquake interseismic velocity of the CNBA station. The red component shows an increase of 6.1 ± 0.2 mm/yr. It is interesting to see that the blue component shows the postseismic slow movement away from the fault, a feature also observed after the 2003 Tokachi-oki earthquake (Fig. 7d). The stations in Fig. 8b and c showing enhanced landward velocities, including CNBA, suffer from data gaps up to two years. Additional time series of two stations are given in Figs. A5. Change in seismicity in the region showing enhanced landward movements are discussed in Section 5.2.

4.4. The 2014 Iquique Earthquake (M_w 8.2)

The 2014 April Iquique earthquake occurred at a segment near the Peru-Chile border. This segment has been known as the north Chilean seismic gap with the last rupture by the 1877 Iquique earthquake (M_w 8.6) (Kelleher, 1972). Postseismic trenchward movements occur near the ruptured fault as the combined effect of the afterslip and the viscoelastic relaxation (Hoffmann et al., 2018). Fig. 9a suggests that the stations located to the south of 21S, as well as one station AREQ to the north, are not affected by such postseismic trenchward movements.

Fig. 9d shows the SRGD station to the south of the rupture, showing small landward velocity increase of 2.8 mm/yr by the 2014 earthquake. On the northern side, AREQ shows the increase of 1.6 mm/yr (Fig. A6). Both SRGD and AREQ stations are located at distances comparable to the fault length from the SE and NW edges of the fault.

Large interplate earthquakes occurred recently around the 2014 Iquique earthquake. To the north, the southern Peru earthquake (M_w 8.4) occurred near Arequipa in 2001, being followed by postseismic deformation continuing for at least two years (Perfettini et al., 2005). The rupture area of the 2001 earthquake seems to be coupled again a decade after the earthquake (Villegas-Lanza et al., 2016). We expect that the increasing of landward velocity at AREQ station after 2014 was not much influenced by the decay of the postseismic movement of the 2001 event.

To the south, the 2007 Tecopilla earthquake (M_w 7.7) (Schurr et al., 2012) and the 1995 Antofagasta earthquake (M_w 8.1) (Pritchard et al., 2002) did not significantly change the slip deficit in the studied region. Strong interplate coupling is confirmed in the 2014 Iquique earthquake focal region prior to the earthquake (Métois et al., 2013; Li et al., 2015). Hence, we think the influences from the postseismic movements of these earthquakes to the landward velocity change following the 2014 Iquique earthquake are small.

4.5. The 2007 Bengkulu Earthquake (M_w 8.4)

The 2007 September Bengkulu earthquake occurred within the southern Sumatra subduction zone as the result of the oblique convergence of the Indo-Australian and the Eurasian plates. This region has been suffering from recurrent large earthquakes for a long time, with a series of large interplate earthquakes occurring since the 2004 December Sumatra-Andaman earthquake (M_w 9.2). Such earthquakes include the 2005 March Nias earthquake (M_w 8.5), the 2007 Bengkulu earthquake (M_w 8.4), and the 2010 Mentawai tsunami earthquake (M_w 7.9). In the past, similar megathrust earthquakes may have hit this area in 1797 and 1833 as inferred from studies of coral microatolls (Natawidjaja et al., 2006). We use the GNSS data of the MLKN station, one of the SuGAR (Sumatra GPS Array) station in the Enggano Island, to compare the velocity before and after the 2007 earthquake.

As seen in Fig. 10a, stations on the rupture and on the northwestern segment show large trenchward postseismic movements. On the other hand, MLKN shows northeastward velocity change by the 2007 earthquake. An unusual situation for this station is that its interseismic velocity is not in the direction of the subduction. As seen in Fig. 10b and c, which compare velocities before and after the 2007 earthquake, the station moves northwestward. This reflects the continuation of the postseismic movement of the 2000 Enggano earthquake (M_w 7.9), whose fault plane is indicated with a red rectangle (Abercrombie et al., 2003). In spite of this situation, the velocity change of MLKN in 2007 coincides with the plate subduction direction. Hence, we think it an example of the postseismic landward velocity changes studied here. The end of the postseismic period is taken at 2010.81, the occurrence time of the Mentawai earthquake, a M_w 7.9 typical tsunami earthquake that occurred close to the 2007 rupture (Satake et al., 2012). MLKN clearly shows the increase of the landward velocity at this segment.

We found the velocity change in the trench-normal component of 5.1 mm/yr following the 2007 Bengkulu earthquake (Fig. 10d). Unlike other cases, MLKN is located quite close to the southeastern edge of the fault of the 2007 earthquake. In this earthquake, the afterslip occurred mainly in the northwest part of the fault, which made the postseismic signals weak at MLKN. Lubis et al. (2013) calculated postseismic crustal movements of the 2007 earthquake by the viscoelastic relaxation, and the results showed insignificant movement around the MLKN station, and this support our interpretation that the velocity change of MLKN comes from the landward increased velocity of the 2007 earthquake.

This region is thought to be a part of the Sunda Strait seismic gap. Mignan et al. (2006) suggested that this area has remarkable accelerated seismic moment release similar to the area where maximum slip occurred during the 2004 Sumatra-Andaman earthquake. Hanifa et al. (2014) pointed out that the region off the southwestern coast of Java is a seismic gap with a high probability of future earthquakes. The enhanced coupling after the 2007 Bengkulu earthquake might contribute to accelerated strain accumulation in those segments.

4.6. The 2012 Oaxaca Earthquake (M_w 7.4)

Recurrent large earthquakes in southern Mexico are due to the subduction of the Cocos plate beneath the southernmost part of the North American plate along the Middle America Trench. Several significant earthquakes occurred in the region near the 2012 March Oaxaca earthquake, e.g. the 1932 M_w 7.9 earthquake, the 1995 M_w 8.0 earthquake, and the 1985 M_w 8.1 earthquake (Kanamori et al., 1993; Courboulex et al., 1997). For this earthquake, we could find only one station suitable for the present study, the OXPE station, (Figs. 11a,b) with meaningful time span before and after the earthquake near the 2012 rupture. Our result showed a small increase of the landward component of the horizontal velocity of 4.1 mm/yr (Fig. 11c). This station is located at a distance comparable to the fault length from the SE edge of the fault.

It is difficult to know if earthquakes before the 2012 Oaxaca earthquake influence landward velocity change because of the lack of enough GNSS data. The last major earthquake that occurred near the OXPE station, is a 1999 M7.5 earthquake (Segou and Parsons, 2018). Considering the time between the two earthquakes, the decay of its postseismic crustal deformation would not significantly influence the results shown in Fig. 11.

5. Discussion

5.1. Overview of the six cases

We reported six cases in four different subduction zones suggesting the post-earthquake occurrence of landward increase of velocity on the segments adjacent along-strike to the ruptured segment. They are not easily explained by conventional interpretations with postseismic processes such as afterslip and local scale viscous relaxation. We first revisited the 2003 Tokachi-oki and the 2011 Tohoku-oki earthquakes in NE Japan reported by Heki and Mitsui (2013). We then studied the 2010 Maule earthquake, Chile, for which Melnick et al. (2017) reported increased landward movements north of the rupture. We also studied the velocity changes associated with the 2014 Iquique earthquake in northern Chile, originally found by Hoffmann et al. (2018). We newly

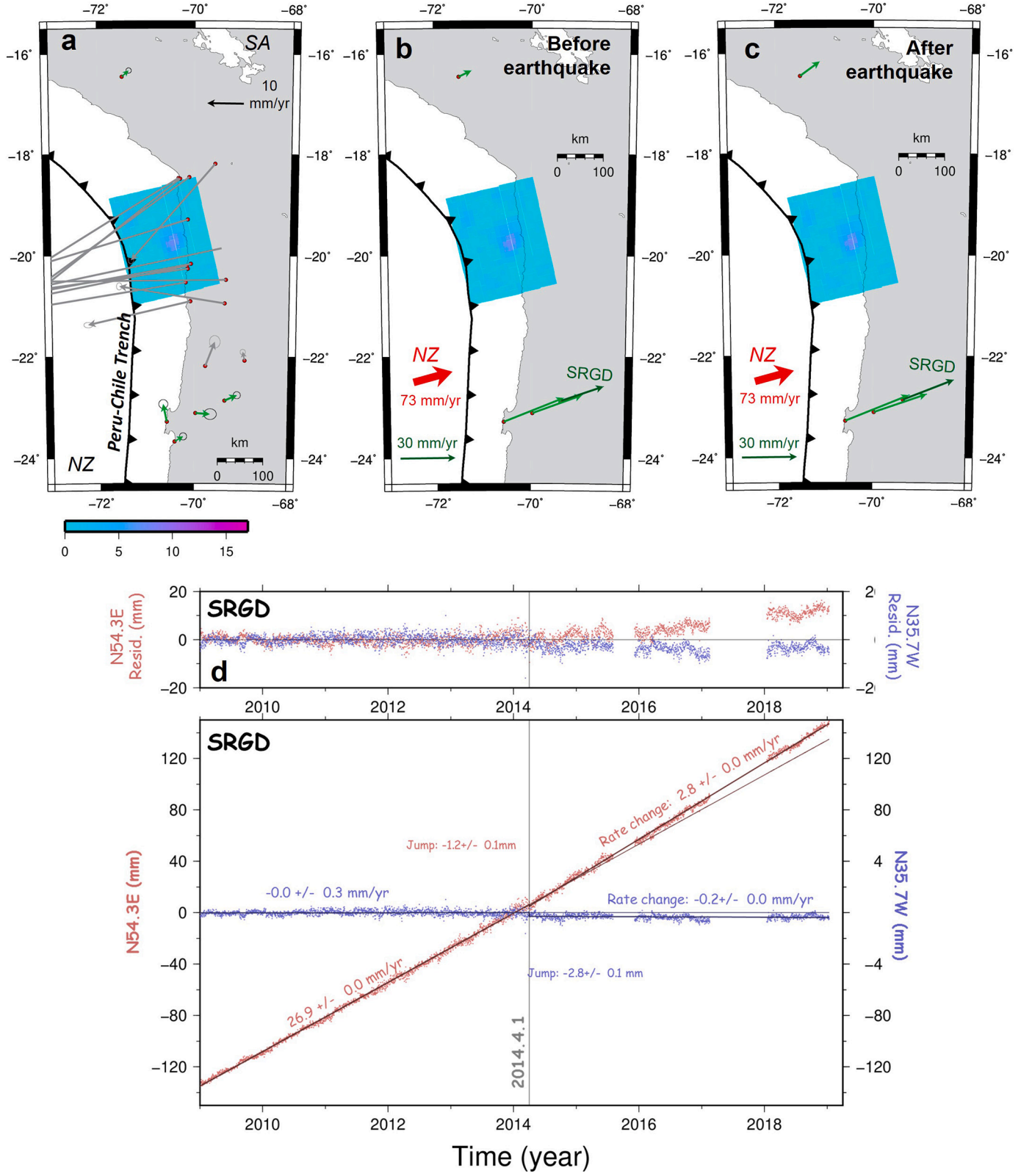

Fig. 9. Maps and diagram demonstrating the postseismic landward velocity changes to the north and south of the 2014 Iquique earthquake rupture. (a) indicates the differences of the velocities before and after the earthquake shown in (b) and (c), respectively. The red arrow represents the Nazca plate movement relative to the South American plate. The time series of the SRGD station (dark green arrow in b, c) are shown in (d) in the trench-normal (red) or trench-parallel (blue) components. (For interpretation of the references to colour in this figure legend, the reader is referred to the web version of this article.)

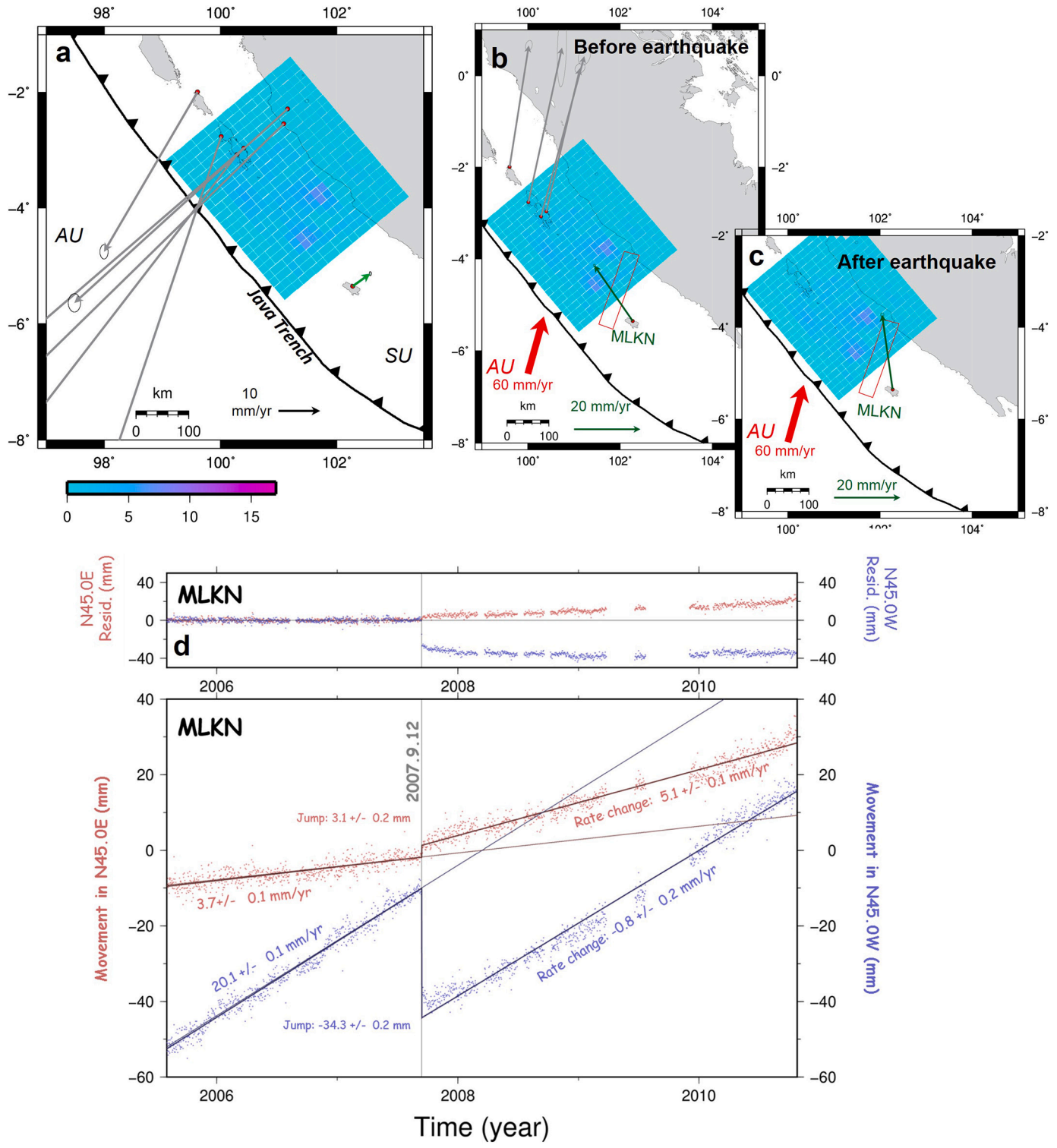

Fig. 10. Maps and diagram showing the increased landward velocity after the 2007 Bengkulu earthquake. (a) Differences of the velocities (relative to the Sunda plate) between periods before and after the earthquake shown in (b) and (c), respectively. The red arrow represents the Australian plate subduction relative to the Sunda plate. The red rectangle indicates the fault plane of the 2000 Enggano earthquake (M_w 7.9). The time series of the MLKN station is shown in (d) using the horizontal directions parallel with (red) or perpendicular to (blue) the subduction direction. (For interpretation of the references to colour in this figure legend, the reader is referred to the web version of this article.)

found the signatures for the 2007 Bengkulu earthquake (Southwestern Sumatra), and the 2012 Oaxaca earthquake (Mexico).

The six examples include the two cases, 2011 Tohoku-oki and 2007 Bengkulu earthquakes, where interseismic velocities deviate largely from relative plate subduction directions. Such deviations are due to long-lasting postseismic crustal movements of past earthquake, i.e. 2003 Tokachi-oki and the 2000 Enggano earthquakes, respectively. Even in these cases, the velocity changes nearly align with the plate subduction directions. We also carefully evaluated the leakage of the decaying trenchward postseismic crustal movements of past large nearby

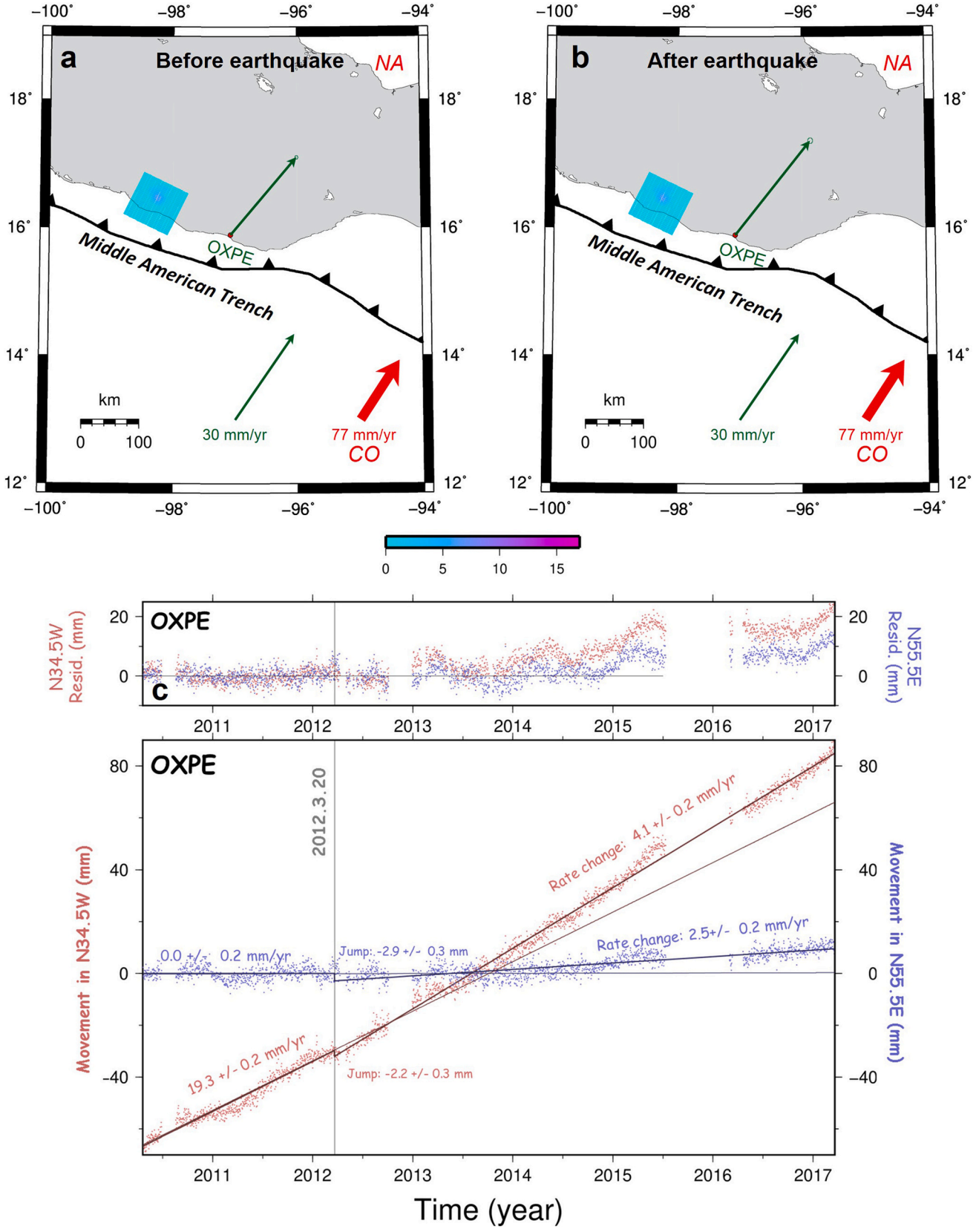

Fig. 11. Maps and diagram demonstrating the postseismic landward velocity increase for the 2012 Oaxaca earthquake. In (a) and (b), we compare the velocity before and after the 2012 earthquake for the station OXPE showing possible postseismic enhanced coupling. The red arrow represents the Cocos plate movement. The velocity vectors are all relative to the North American plate. The time series of the horizontal coordinates of the OXPE station (dark green arrow in a, b) is shown in (c) using the components parallel with (red) or perpendicular to (blue) the subduction direction. (For interpretation of the references to colour in this figure legend, the reader is referred to the web version of this article.)

earthquakes into the inferred landward velocity increases.

In addition to landward velocity increase, a trench-parallel velocity change was found after the 2003 Tokachi-oki earthquake. Also, in the 2010 Maule earthquake, the changes of the velocities are somewhat deviated counterclockwise from the plate subduction direction (Fig. 8a). Such changes could be driven by postseismic viscous relaxation. Vertical velocities may also have changed at stations showing enhanced landward velocities. Because of the larger noises in vertical component, we cannot draw decisive conclusions for them (Fig. A2). We will revisit the problem after we obtain data with enough time span.

In addition to the six cases studied here, we looked for similar increase signatures for other megathrusts in various subduction zones. They include the 2004 December Sumatra-Andaman earthquake (M_w 9.2) and the 2005 March Nias earthquake (M_w 8.6) (Fig. 1). We were unsuccessful in these cases simply due to the lack of enough time span of pre- and postseismic data from GNSS stations in appropriate places. The movements of the SuGAR stations are well documented by e.g., Feng et al. (2015). Below we summarize the situation.

The three SuGAR stations (PSMK, PTLO, PBAI) in islands to the northwest of Sumatra started working well before the 2004 earthquake and may have recorded enhanced landward velocities following that event. However, the 2005 March earthquake occurred before we can confirm its signature, and their velocity changed trenchward due to the postseismic movements by the 2005 event. Three SuGAR stations (MSAI, PSKI, BSAT) off the middle Sumatra started operation before 2004, but they were not close enough to the 2005 rupture and did not show significant post-2005 landward velocity change. We think it likely that these two earthquakes caused landward velocity increases in this subduction considering possible triggering of earthquakes in adjacent segments (Haridhi et al., 2018), e.g., the 2005 Nias earthquake to the southeast of the 2004 Sumatra-Andaman earthquake, and the 2010 Mentawai earthquake and the 2007 Bengkulu earthquake further to the southeast. It is a pity that we could not confirm this by geodetic data.

A similar situation applies for the 2015 Illapel earthquake (M_w 8.3), in central Chile (Fig. 1). For example, the COPO station is in the region suitable to study increased coupling by the 2015 earthquake, but its observation data are not available after 2015.

5.2. Increased seismicity

If such a landward velocity change in the neighboring segments of the megathrust ruptures is related to the enhanced trench-normal shortening rate, shear stress buildup would also increase there. To confirm this as increased seismic activity (Uchida et al., 2016; Ide, 2013), we compared seismicity before and after the megathrust earthquakes in those segments (Figs. 12, A8, A9).

Increased seismicity right after the 2011 Tohoku-oki in the Pacific coast of eastern Hokkaido is difficult to confirm. This is due to the temporary increase of seismicity that started a few years before the 2011 earthquake (gray region in Fig. 12c). This increase is not due to aftershocks because of the lack of significant earthquakes in this period (Fig. A8). This increase is considered an artifact (K. Katsumata personal comm. on 2020/9/11) with possible origins including the change in detection capability (Habermann, 1991), natural change in background

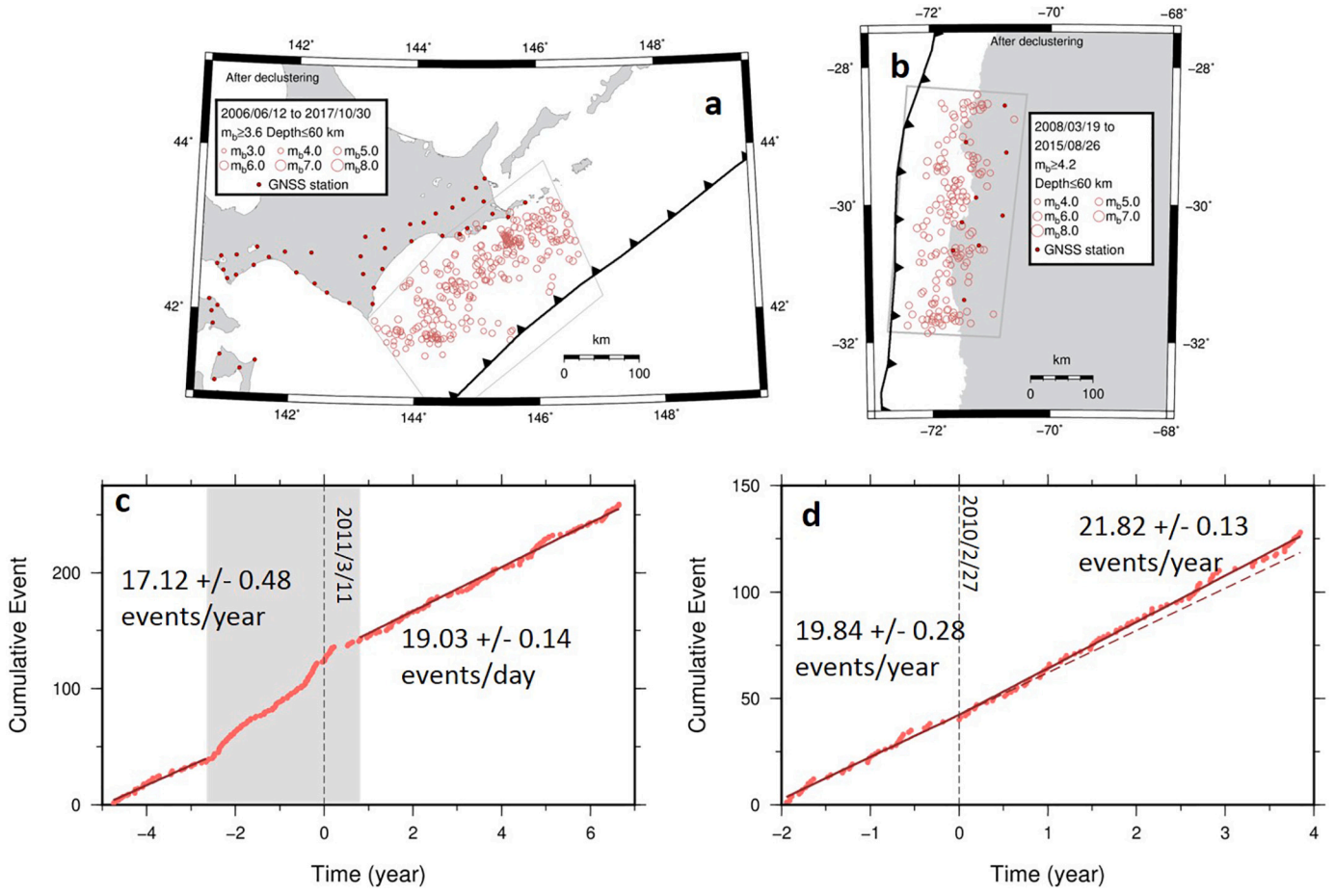

Fig. 12. The change in seismicity in the Pacific coast region in eastern Hokkaido (a, c) and near the Pacific coast of central Chile (b, d) in the region showing increased landward velocities following the 2011 Tohoku-oki earthquake and the 2010 Maule earthquake, respectively. The vertical dashed lines (c, d) indicate the earthquake occurrence times. We used the period from 2006/06/12 to 2017/10/30 for the Tohoku-oki case and 2008/03/26 to 2015/08/26 for the Maule case. Gray zone (c) shows the period of increased background seismicity by an unknown origin.

seismicity (background fluctuation), and the ETAS problem itself (Lombardi et al., 2010). Here we shifted the periods before and after the 2011 earthquake to exclude the gray area in Fig. 12c. This let us see the increase in seismicity possibly caused by the enhanced coupling associated with the 2011 Tohoku-oki earthquake (Fig. 12c).

Figs. 12d shows the increase of seismicity from the two- and four-year periods before and after the 2010 Maule earthquake, respectively, within the rectangles shown in Fig. 12b. There we show the number of earthquakes, and we can see an increase in seismicity of ~10%, which is smaller than the rate of increase in landward velocity (~20% in CNBA, see Fig. 8). In both the Japanese and Chilean cases, the rates of the seismicity increases are not so high as those in the rates of the increased landward velocities.

5.3. Spatial decay of the enhanced coupling

The enhanced coupling may encourage future failures in the neighboring segments. For example, earthquakes such as the 2015 Illapel earthquake (M_w 8.3) and the 2016 Chiloé earthquake (M_w 7.6), occurred to the north and south of the 2010 Maule earthquake, respectively, may

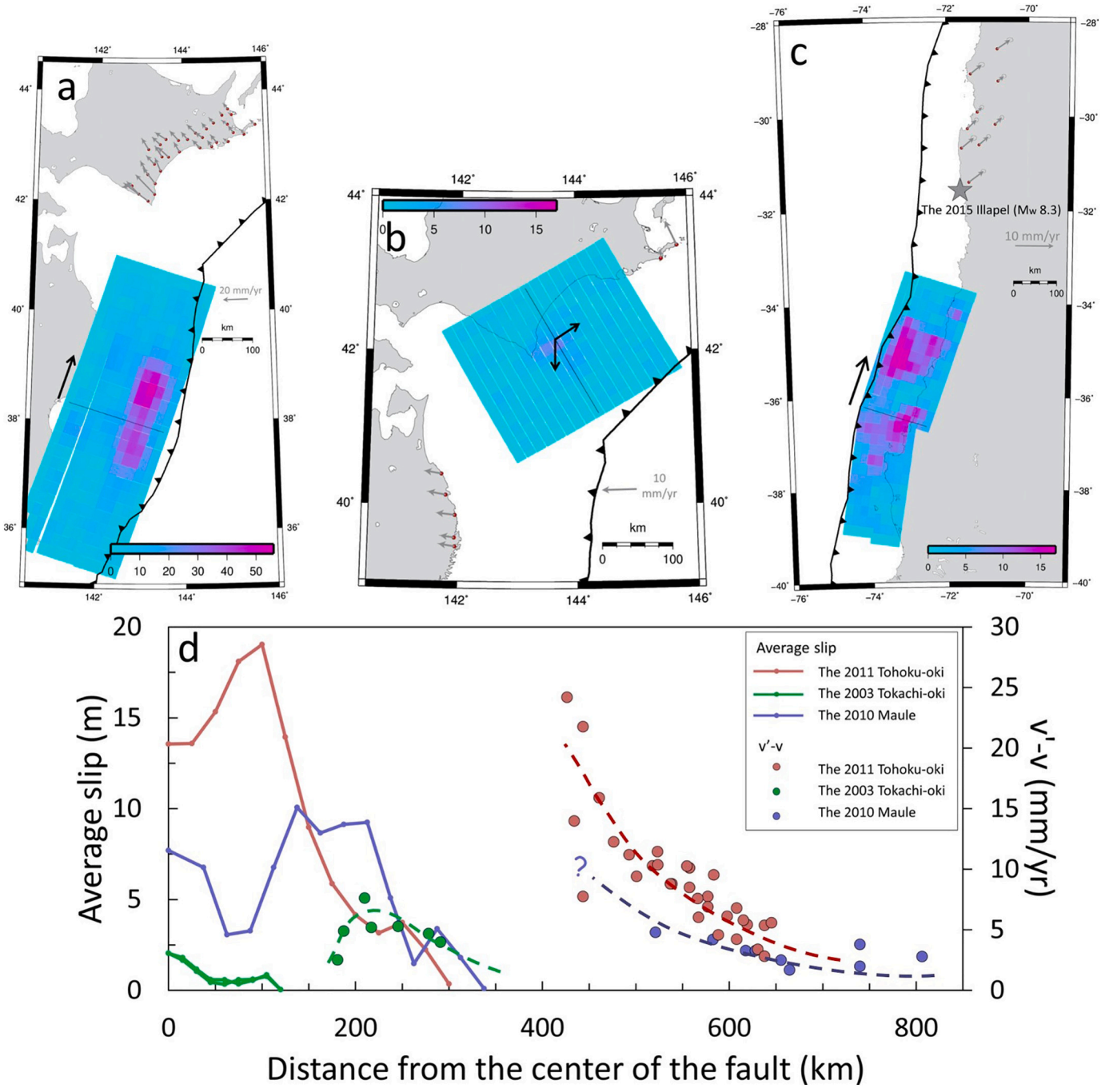

Fig. 13. Dependence of the increase of landward velocities (v'-v) of forearc stations on the distance from the center of the fault for the 2011 Tohoku-oki, the 2010 Maule, and the 2003 Tokachi-oki earthquakes. The distance was calculated in the direction of fault strike (black arrows), except for the south of the 2003 Tokachi-oki case due to the bending of the trench (d). We included data from ~30 GNSS stations near the Pacific coast of Hokkaido (a), 7 stations near the Pacific coast of NE Japan and Hokkaido (b), and 9 stations near the pacific coast of central Chile (c). The average slips in both along-strike directions from the fault centers are obtained from the slip models from USGS. Broken curves are hypothetical smooth models.

have been triggered by the enhanced coupling caused by the 2010 Maule event (M_w 8.8) (Melnick et al., 2017; Ruiz et al., 2017). To further discuss this issue, it is important to know the spatial and temporal decay of the enhanced coupling.

In Section 4, we did not pay much attention to the relationship between amounts of the velocity changes and distances from the ruptured faults. In Fig. 13, we plot the landward velocity increases as a function of the distance from the center of the fault for the 2003 Tokachi-oki, 2011 Tohoku-oki, and the 2010 Maule earthquakes. For the Tohoku-oki case, postseismic trenchward movements seem to prevail from the rupture area as far to the northeast as ~100 km from the fault edge. According to the slab acceleration model (Section 3), this does not mean the absence of slab acceleration there. The acceleration is the largest just beneath the ruptured fault, but it is "hidden" by the oceanward movement of the forearc caused by the afterslip and viscoelastic relaxation.

For the 2011 Tohoku-oki case, the landward velocity changes prevail for stations farther than ~100 km from the fault edge. Such an increase is confirmed to continue as far as ~650 km from the fault center, but it is not clear if it extends beyond that point due to the lack of data. For the 2010 Maule case, we have data only beyond 500 km from the fault center. Probably, the true maximum landward velocity increase for this event would exist somewhere with distance <500 km. For this earthquake, the data are available as far as 800 km, and the velocity increases seem to decay gradually for distance range 500–800 km. For the 2003 Tokachi-oki case, landward increase appears in the stations closer to the fault, and its maximum occurs only ~100 km from the fault edge. From these three cases, the landward velocity increase seems to extend at least as far as ~1/2 the fault lengths beyond the fault edges.

If such a landward velocity increase is associated with the increased interplate coupling, large earthquakes may be encouraged in the future in "affected segments," e.g., the southern Kuril Islands and central Chile. It would be reasonable to consider that the enhanced interplate coupling to the north of the Maule rupture has triggered the 2015 M_w 8.3 Illapel earthquake (see Fig. 13c for position). Luo et al. (2020) recently proposed that the 2010 Maule and the 2016 Chiloé earthquakes might be related to the enhanced coupling starting a few years prior to 2010 in the rupture area of the 1960 Chile earthquake. This suggests spatial and temporal complexity of the triggering problem.

D'acquisto et al. (2020) used the velocity-driven 3D mechanical finite element models to quantify and analyze the deformation that produces landward motion by the viscous relaxation of the mantle wedge and the deep afterslip. Their results show increased postseismic landward motion of up to ~6.1 mm/yr at (trench-parallel) distances >450 km from the middle of the ruptured asperity. They conclude that enhanced landward motion is generated by in-plane elastic bending of the overriding plate and mantle wedge in response to oceanward motion of lithosphere around the rupture zones. Their results are also consistent with the observations in Central Chile. Melnick et al. (2017) used a large-scale three-dimensional thermomechanical model to simulate viscoelastic relaxation of the mantle to explain continental-scale velocity changes. Their model also reproduces the observed landward velocity increase.

5.4. Temporal decay of the enhanced coupling

Another important aspect is the temporal decay. According to the slab acceleration model (Section 3), The enhanced coupling decays as the interplate coupling *Fc* returns to the pre-earthquake state. Such a recovery time may depend on the earthquake magnitude, i.e. the larger the magnitude, the longer the period for the recovery of interplate coupling. In the time series of trench-normal movements (Figs. 6-11), temporal decays are not very evident, i.e. landward movements show

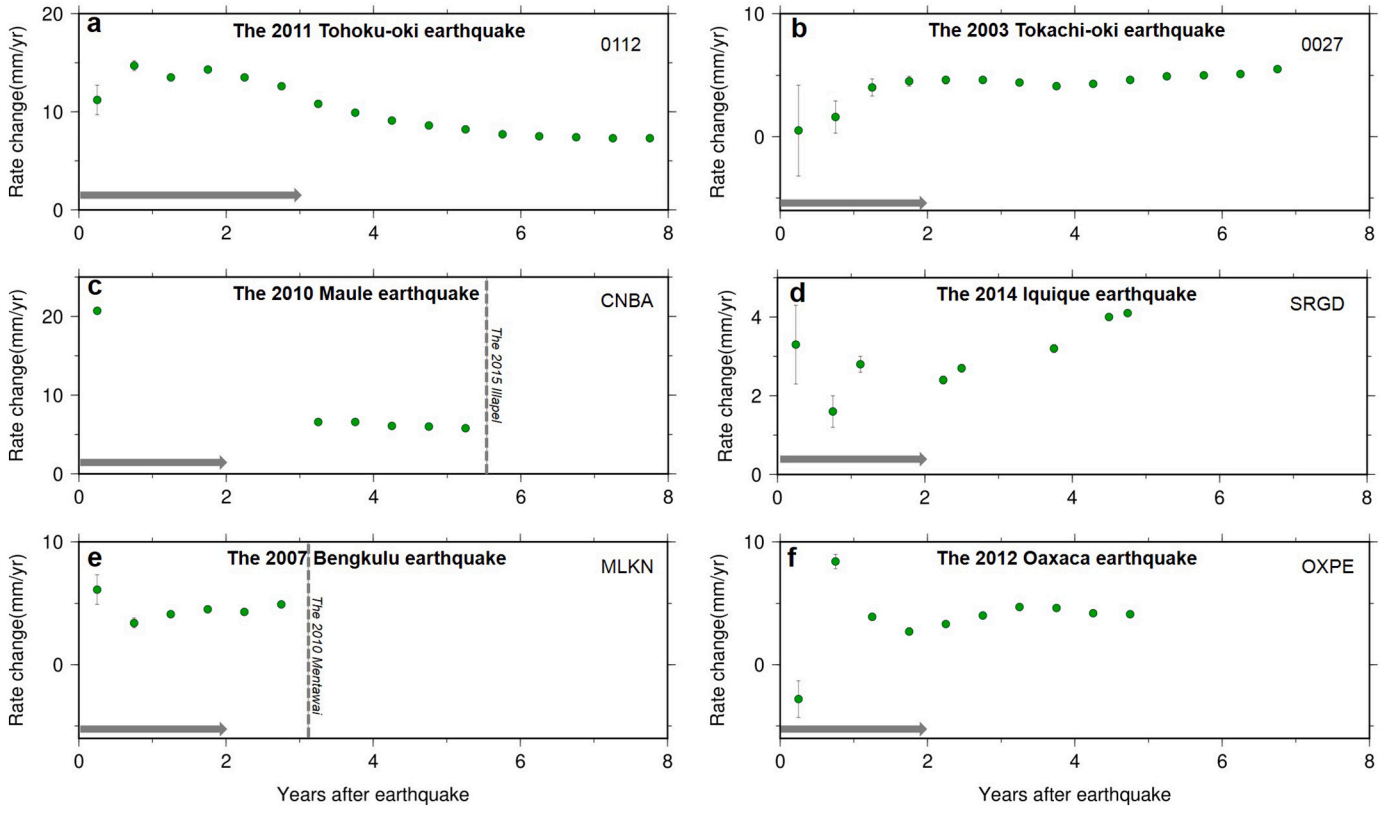

Fig. 14. Interseismic landward velocity change estimated within moving 1-year time windows (a-f). Horizontal coordinates of the green circles show the centers of the time windows. Gray arrows represent the duration of postseismic decay based on previous studies. In (c) and (e), we exclude data after significant earthquakes occurred nearby (black dashed line). After periods of instability, the rate becomes stationary for subsequent years. In the two Chilean cases (c, d), data gaps make the rate change unstable. (For interpretation of the references to colour in this figure legend, the reader is referred to the web version of this article.)

simple increased linear trends without notable curvatures. Here we confirm this numerically.

We set up the moving 1-year time period for the linear regression to see possible temporal change in slope (Fig. 14). This analysis shows that velocity changes are either higher or lower in the first few postseismic years due to postseismic transients. Gray arrows in Fig. 14 indicate rough length of significant postseismic transients given in past literatures. After these years, the velocity changes seem to remain stable.

Fig. 15 presents an example of a long-time continuous distance changes of a baseline in Hokkaido, connecting the 0010 and 0102 stations. This baseline is approximately in the direction of the Pacific plate subduction and the data covers from 1996 to 2020. The distance gets shorter as the interseismic compressive strain accumulates. This is disrupted by two interplate earthquakes in 2003 Tokachi-oki (M_w 8.3) earthquake and the 2004 Kushiro-oki (M_w 7.0) earthquake (Tanioka and Katsumata, 2007). After a few years of oceanward movement of 0010 (increase of the distance), distance resumed to decrease. The rate before and after these two earthquakes are 29.3 mm/yr and 27.5 mm/yr, respectively. After the 2011 Tohoku-oki earthquake, this rate increased to 32.9 mm/yr due to the enhanced landward movement of 0010.

An important feature in Fig. 15 is that the increased landward velocity does not seem to decay in time up to now. It shows temporary enhanced shortening for two years. After that, the baseline continues to contract at a steady increased rate up to now. Yamagiwa et al. (2015) showed that afterslip has mostly decayed in 2.5 years, while viscous relaxation continues over a longer time with a time constant of ~10 years. The increased landward velocity as seen in Fig. 15 would have a longer time constant. As already mentioned in Heki and Mitsui (2013), such an apparent lack of decay is a striking feature of this phenomenon, and we need observations over longer time windows to understand the process.

5.5. Forearc station velocities and slab velocities

Heki and Mitsui (2013) hypothesized that postseismic enhancements of the interplate coupling may reflect the accelerated rate of the slab subduction u'-u in response to the modified balance of forces acting on the subducting slab (Fig. 5). Actually, what we observe is the change in velocity of forearc GNSS stations v'-v, and we need to convert v'-v to u'-u. Generally, v becomes larger if interplate coupling is stronger, but v never exceeds u. We here inferred the ratio v/u ($0 \leq v/u < 1$) by comparing the observed interseismic velocity of the GNSS station and the subduction speed calculated by the MORVEL model (Argus et al., 2011).

For example, in the Maule earthquake, the velocity of the CNBA station observed before (v_{CNBA}) and after (v'_{CNBA}) the earthquake, is related to the hypothetical slab acceleration u'_{Nazca}-u_{Nazca}, using the subduction speed of the Nazca plate v_{Nazca} relative to the South American plate at the Chile trench, as follows,

$$u'_{Nazca} - u_{Nazca} = (v_{Nazca}/v_{CNBA}) \times (v'_{CNBA} - v_{CNBA}) \quad (6)$$

This conversion is applied to all cases except the Tohoku-oki and the Bengkulu earthquakes. In these two cases, postseismic movements of nearby earthquakes in recent past still influenced v and v' (Figs. 6 and 10), i.e. the 2003 Tokachi-oki and the 2000 Enggano earthquakes, respectively. In Japan, we used the interseismic velocities before the earlier earthquake (i.e. before 2003). For the MLKN station, the data are not available before 2000, and so we used the average of interseismic velocities in 2000–2007 of the five stations above the 2007 rupture (Fig. 10a) to infer v_{MLKN}.

By such calculations, the acceleration of the slab subduction for the six cases became, 22.0 mm/yr (2011 Tohoku-oki), 8.4 mm/yr (2003 Tokachi-oki), 10.4 mm/yr (2010 Maule), 6.6 mm/yr (2014 Iquique), 8.5 mm/yr (2007 Bengkulu), and 10.1 mm/yr (2012 Oaxaca). For the first four cases, we have data from multiple stations and calculated the uncertainties in such velocity changes.

5.6. Comparison of the data with the slab acceleration model (Heki and Mitsui, 2013)

Here we examine the slab acceleration model by Heki and Mitsui (2013) by comparing the acceleration of the subduction speed inferred in the previous section with the model predictions. The eq. (2) suggests that the decrease in the coupling F_c'-F_c determines the slab acceleration u'-u. The acceleration would hence depend on M_w, because a larger earthquake would cause larger F_c'-F_c. Fig. 16 compares de-trended time series of trench-normal movements of the forearc stations for the six cases studied here, using a unified vertical axis. The figure shows that the acceleration is larger for a case with a larger M_w, and the most significant velocity increase appeared following the M_w 9.0 2011 Tohoku-oki earthquake.

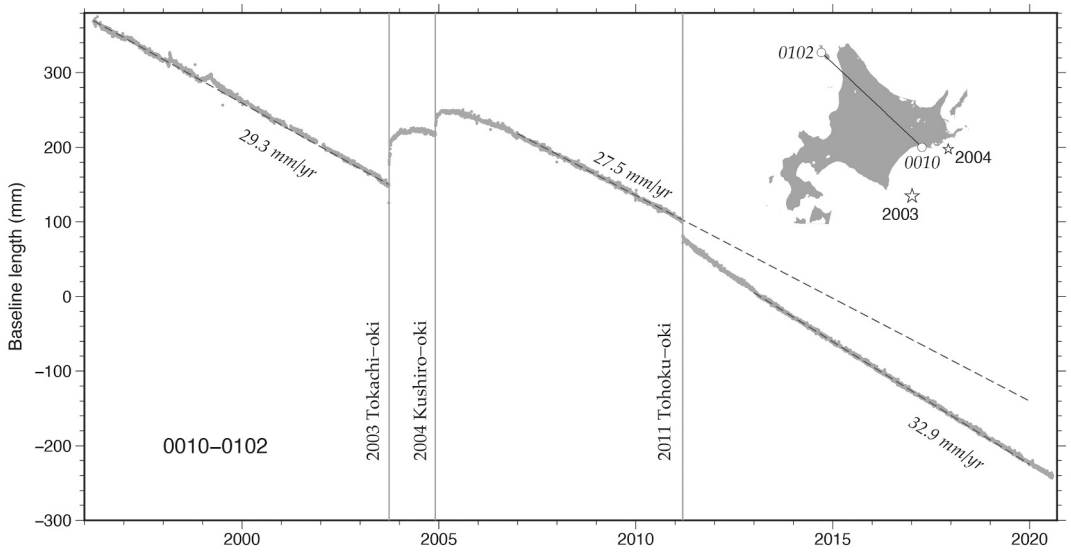

Fig. 15. Time series of the distance between two GNSS stations in Hokkaido, Japan, showing little temporal decay of the landward increased velocity started after the 2011 Tohoku-oki earthquake. The inset map shows the position of the two GNSS stations, and the epicenters of the two earthquakes, 2003 Tokachi-oki (M_w 8.3) and 2004 Kushiro-oki (M_w 7.0) earthquakes. The three rates attached to the dashed lines are average rate for periods 1996.0–2003.74 (29.3 mm/yr), 2007.0–2011.19 (27.5 mm/yr), and 2013.0-now (32.9 mm/yr).

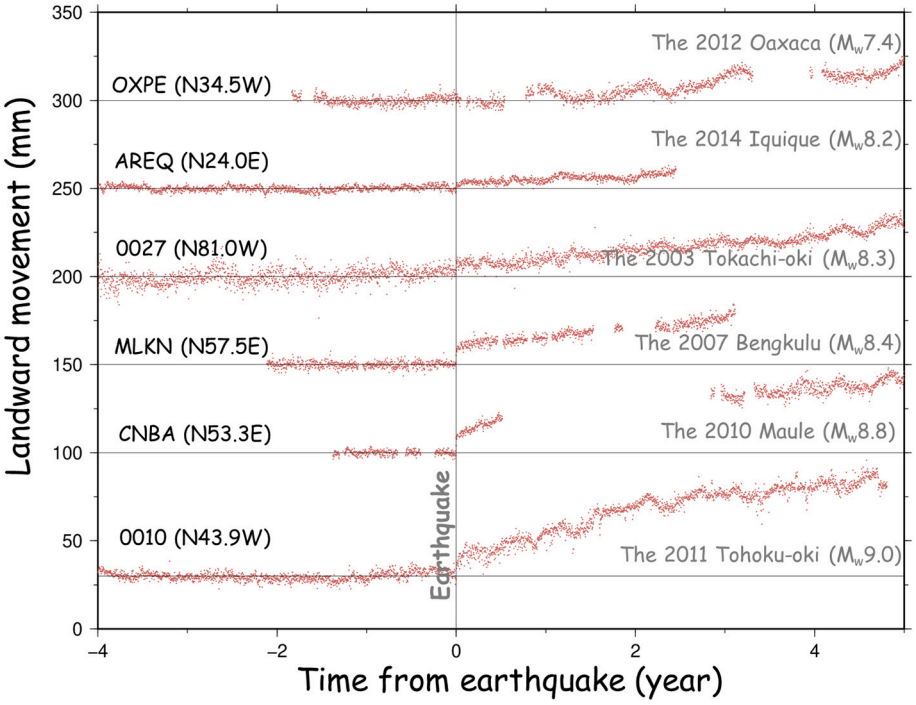

Fig. 16. Comparison of the increased landward velocities of GNSS stations following six megathrust earthquakes studied here. We removed linear trends before the earthquakes to facilitate the comparison of postseismic velocity increases for the six cases. The vertical gray line, used as the origin, indicates the earthquake occurrence times. The station names and the azimuths of the displayed movements are given to the left, and the earthquake names and their M_w are given to the right.

The surface velocity changes *v*'-*v* in Fig. 16 are converted to slab velocity changes *u*'-*u*, as discussed in the previous section. Fig. 17a compares *u*'-*u* in addition to *v*'-*v* as a function of M_w. There, smaller symbols show *v*'-*v* and *u*'-*u* at individual stations for earthquakes where multiple stations are available. We can see that a larger earthquake brings a larger change, both forearc (*v*) and slab (*u*) velocities.

As discussed in Section 3, the loss of coupling *Fc*'– *Fc* would be proportional to the coseismic slip averaged over the fault s_{av} if we fix other parameters. Fig. 17b compares the slab acceleration with the average slip s_{av}, calculated using the slip data of USGS as shown in Figs. 6-11. The acceleration seems to show good correlation with s_{av} considering that the value for the 2010 Maule earthquake is an underestimate (Fig. 13d). However, it is not very clear if the two quantities are proportional considering the four earthquakes with $M_w \leq 8.5$ are clustered at a down-left corner of the figure and do not contribute to the evaluation of the linearity.

Eq. (5) also suggests that the slab acceleration is inversely proportional to *W*, the length the slab surface. Here we assumed that *W* is twice as long as the slab lengths inferred from seismic tomography studies and compare *u*'-*u* and s_{av}/W in Fig. 17c. Here we use the information on the lengths *W*, twice as long as the slab length, i.e. 1075 km for NE Japan (Deal and Nolet, 1999), 1100 km for Chile (Scire et al., 2017), 700 km for Sumatra (Hafkenscheid et al., 2001), and 900 km for Mexico (Husker and Davis, 2009). Noting that the value for the Maule event is underestimated, data in Fig. 17c suggest linearity. Nevertheless, they are not enough to provide a firm support to the slab acceleration model by Heki

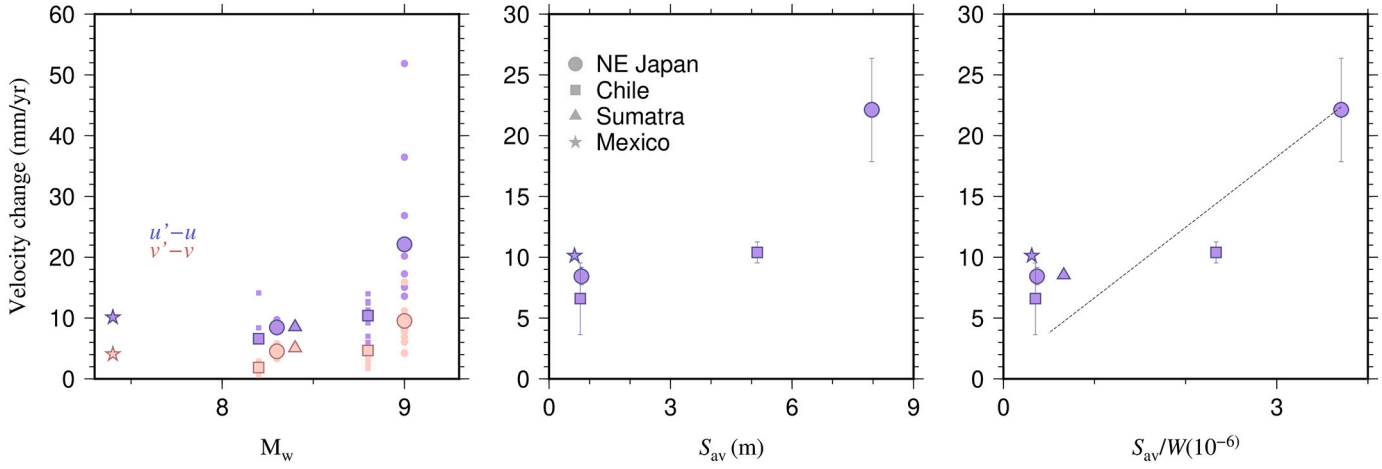

Fig. 17. (a) Comparison of the forearc acceleration, *v*'-*v*, and the slab acceleration, *u*'-*u*, for six different megathrust earthquakes with M_w7.4–9.0. Different symbols indicate different subduction zones. Smaller symbols show values at individual stations for the cases with multiple available stations. (b) M_w is replaced with the slips averaged over the faults (s_{av}) in (b) and with s_{av}/W, where *W* corresponds to the length of the slab surface (see eq. 5). Error bars show the 1σ uncertainties of the averages of these velocity changes.

and Mitsui (2013), considering that 4 smaller earthquakes are clustered and do not fully contribute to the evaluation of the linearity. After all, the data obtained in this study support the model, but they are not strong enough to rule out other possibilities.

The dashed line in Fig. 17c has the slope of 6.1×10^3 yr^{-1}, which corresponds to 1.93×10^{-4} s^{-1}. This slope is equivalent to $\nu d/\mu$ in eq. (5) as the average of the four subduction zones studied here (although the 2011 Tohoku-oki and the 2010 Maule data mainly contribute to the determination of this slope). If we put 50 GPa and 10^{17} Pa s into ν and μ, we get 380 m for d, the thickness of the low-viscosity layer at the slab surface.

6. Conclusions

We compiled GNSS data showing increased landward velocities that occurred in segments adjacent along-strike to six recent megathrust earthquakes in four different subduction zones (Fig. 1). Our results confirmed previous studies for the 2003 Tokachi-oki (Heki and Mitsui, 2013), the 2010 Maule (Melnick et al., 2017), and the 2014 Iquique (Hoffmann et al., 2018) earthquakes. We updated the case of the 2011 Tohoku-oki earthquake, studied briefly in Heki and Mitsui (2013), using GNSS data with longer time span. We found similar landward increase of velocity signatures for three more earthquakes in Sumatra, Chile, and Mexico subduction zones.

From the case of the 2011 Tohoku-oki and the 2010 Maule earthquakes, we found that the landward velocity change extends to the distance comparable to the ruptured fault length (400–500 km) from the fault center (Fig. 13d). Temporal decay was not clear suggesting relatively long-time constants of the phenomenon. We found moderate increase in seismic activities for the two largest earthquakes associated with the increased landward velocities. The velocity change showed a positive correlation with M_w and seems to scale with the average slip. This is consistent with the hypothetical slab acceleration model by Heki and Mitsui (2013) but does not rule out other possibilities. We consider that such landward velocity increase correlates with the enhanced interplate coupling in the adjacent segment, and the increased stress accumulation may encourage future earthquakes in segments influenced by the enhanced coupling, e.g., the eastern Hokkaido.

Declaration of Competing Interest

The authors declare that they have no known competing financial interests or personal relationships that could have appeared to influence the work reported in this paper.

Acknowledgment

This study was funded by Indonesia Endowment Fund for Education (LPDP) PRJ-290/LPDP.3/2016.

Credit author statement

Mohammad Yuzariyadi, Kosuke Heki: Conceptualization, Methodology, Software, Formal analysis, Resources, Data curation. **Mohammad Yuzariyadi:** Investigation, Writing original draft, Visualization. **Kosuke Heki**: Writing Review & Editing, Supervision.

Appendix A. Appendix

A.1. Modeling the station coordinate time series with and without seasonal terms

We subtract the average seasonal components, composed of annual and semiannual terms, in plotting Figs. 6d, 7d, 8d, 9d, 10d, and 11c. In Fig. A1, we show examples of the time series, which compare those with and without average seasonal changes. Such seasonal movements usually originate from seasonal changes of surface loads, and their horizontal components are smaller in amplitudes than the vertical component.

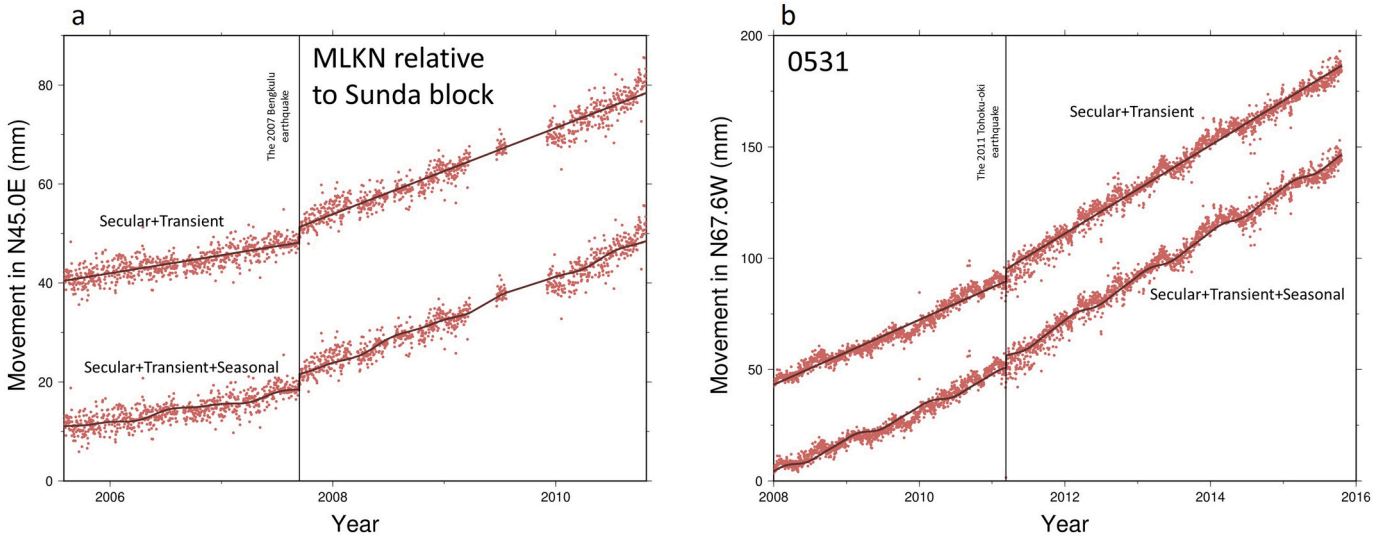

Fig. A1. Landward movement time series of the stations MLKN (Bengkulu, Indonesia) and 0531 (Hokkaido, Japan). Both two time series are modeled considering linear trends (including changes in trends associated with earthquakes), jumps caused by antenna replacements (for GEONET stations), and average seasonal changes. The average seasonal components are removed in the upper time series.

A.2. Trend changes in vertical component

We tried to detect changes in vertical velocities associated with the 2011 Tohoku-oki earthquake. We show them as vectors on the map in Fig. A2a and as time series of two stations in Fig. A2b. They are, however, mostly insignificant and non-systematic. For the 2010 Maule earthquake, due to a

long data gap and large noises, it is difficult to discuss coseismic changes in vertical velocities (Fig. A2c,d).

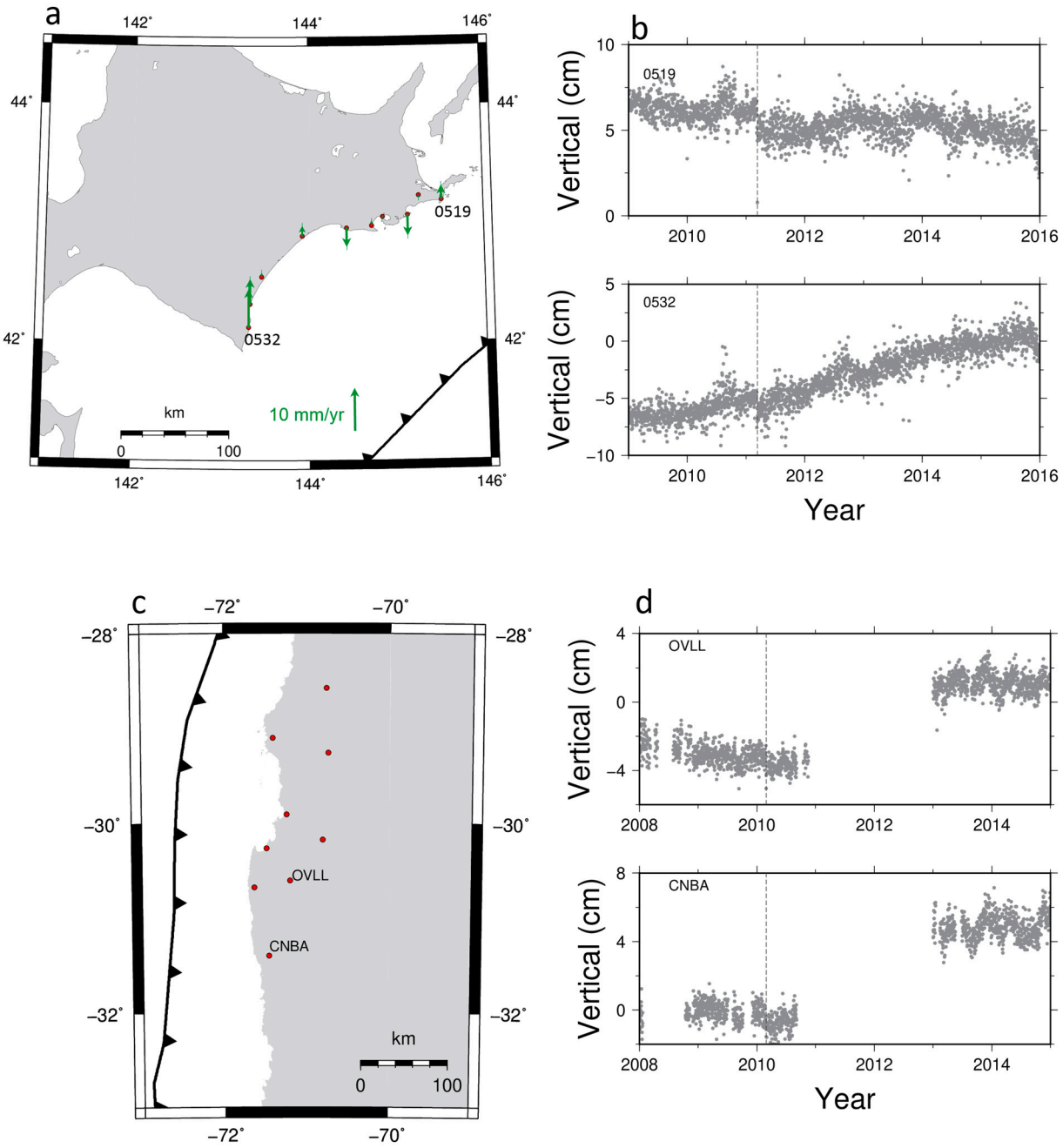

Fig. A2. (a) Vertical velocity changes of GNSS stations in Hokkaido associated with the 2011 Tohoku-oki earthquake. We selected the same periods as in Fig. 6. (b) Time series of the vertical position of the stations 0519 and 0532, shown in (a). (c) We selected two Chilean stations, and (d) plot their vertical position time series before and after the 2010 Maule earthquake.

A.3. Additional time series of horizontal components for 4 earthquakes

In addition to the sample time series in the trench-normal (red) and trench-parallel (blue) components given for Japanese and Chilean cases in Figs. 6d, 7d, 8d, 9d, we show two more examples for each of the earthquakes in Figs. A3, A4, A5, and A6.

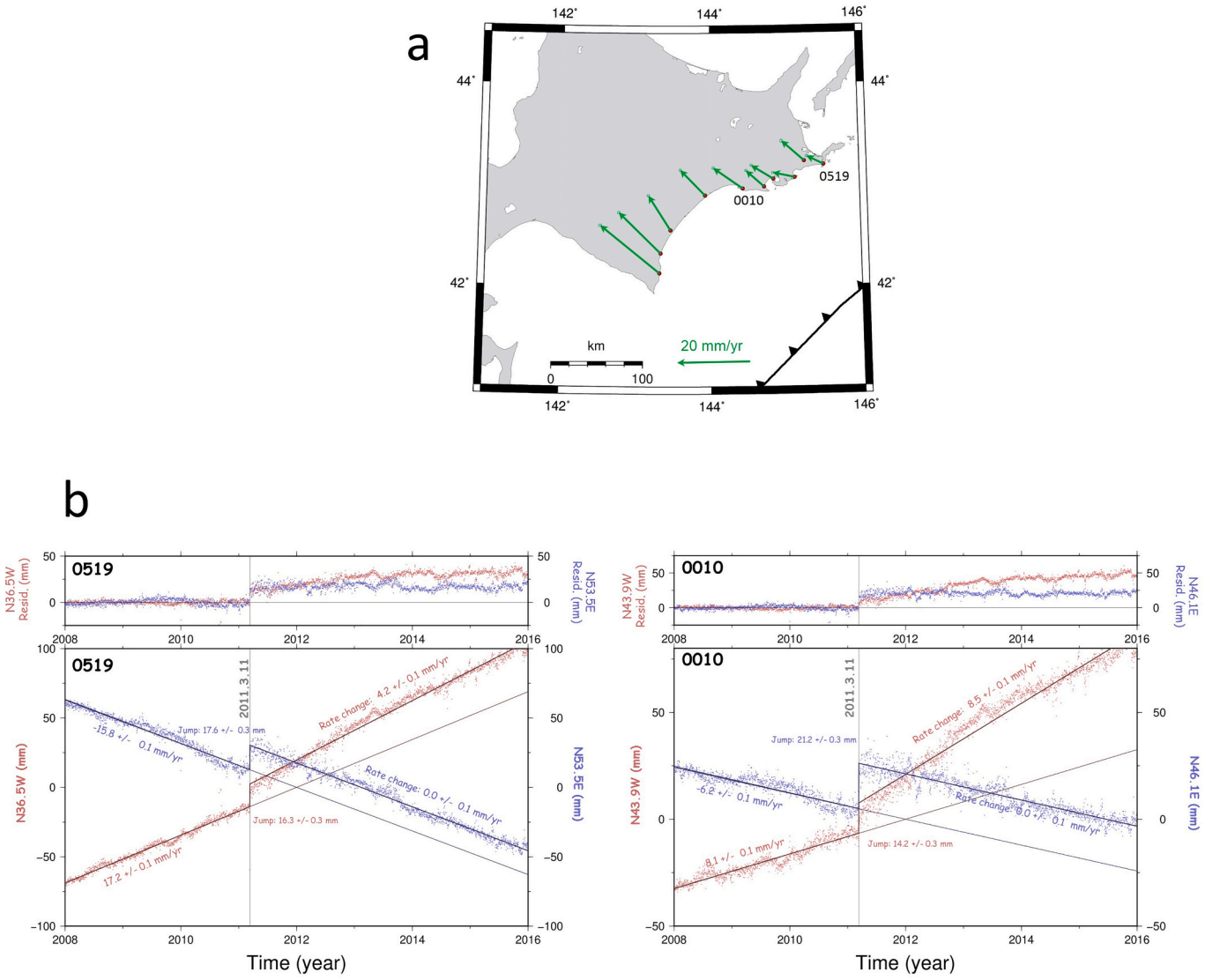

Fig. A3. (a) Horizontal velocity changes associated with the 2011 Tohoku-oki earthquake in Hokkaido (same as stations with green arrows in Fig. 6a). Time series of the two labeled stations (0010, 0519) are shown in (b). The components shown in blue colors are determined as the direction perpendicular to the velocity changes by the earthquake. The components in red are taken perpendicular to them. (For interpretation of the references to colour in this figure legend, the reader is referred to the web version of this article.)

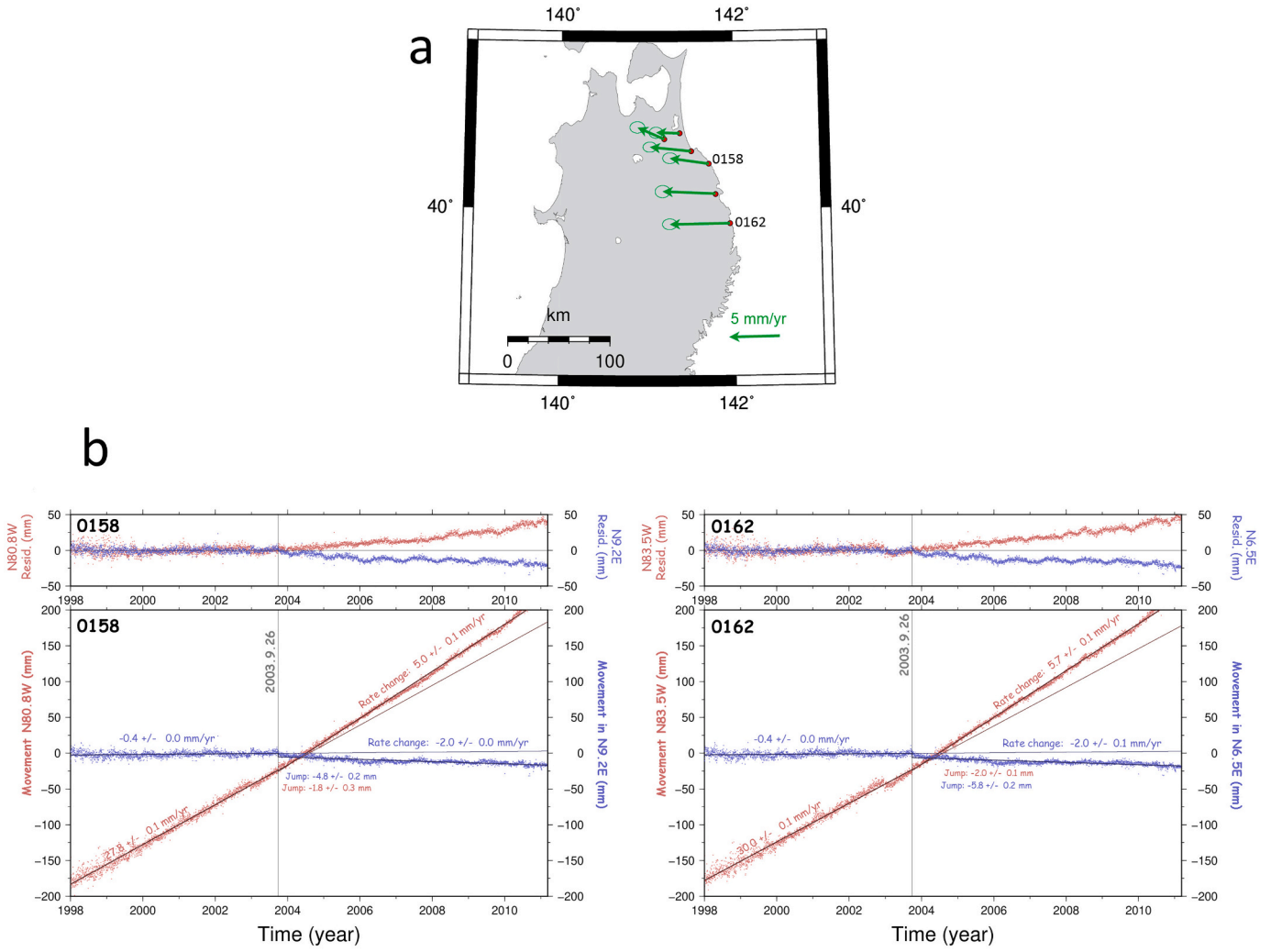

Fig. A4. (a) Horizontal velocity changes associated with the 2003 Tokachi-oki earthquake (same as stations with green arrows in Fig. 7a). In (b), we show time series of horizontal positions of the two stations 0158 and 0162 before and after the earthquake. (For interpretation of the references to colour in this figure legend, the reader is referred to the web version of this article.)

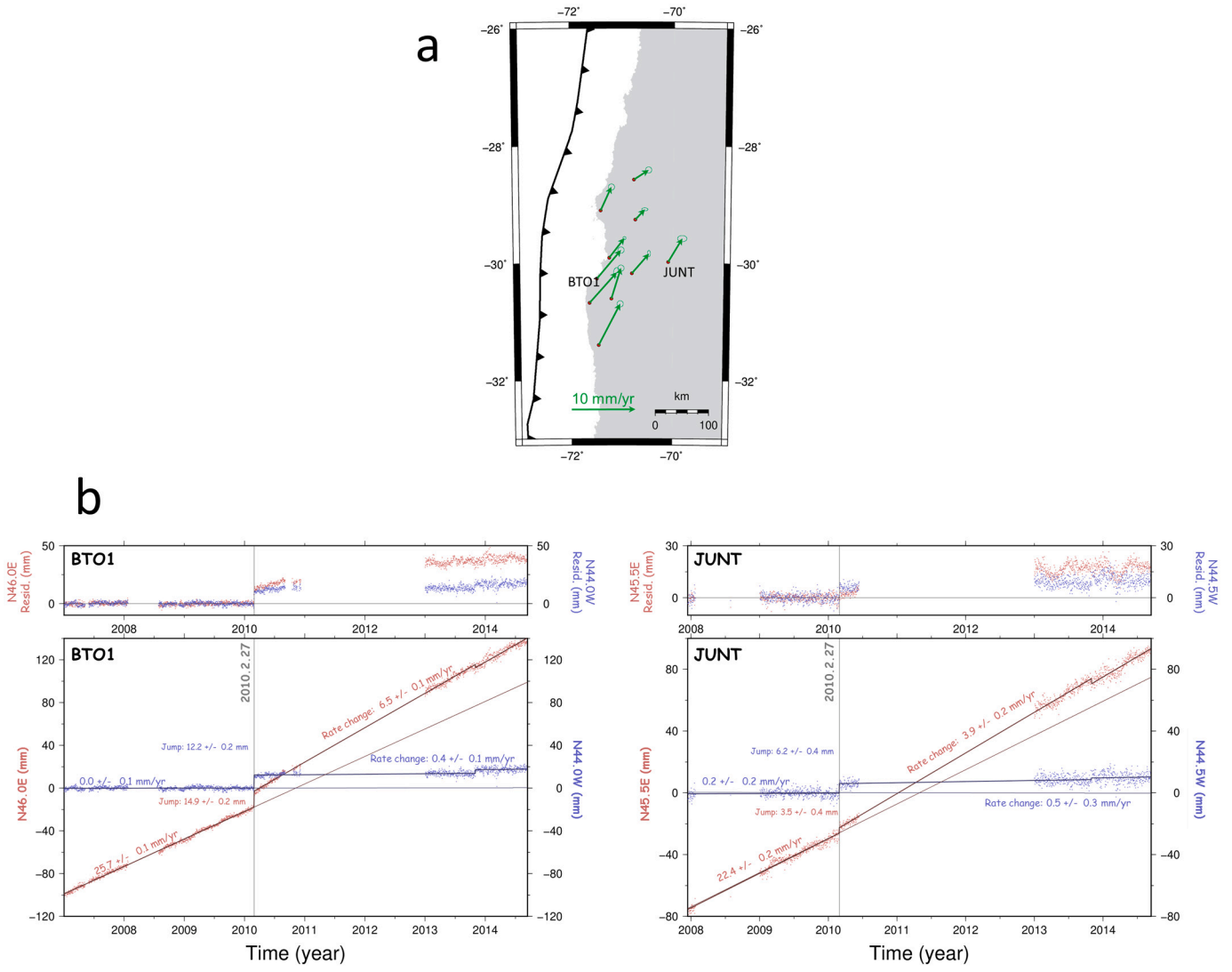

Fig. A5. (a) Horizontal velocity changes by the 2010 Maule earthquake (same as stations with green arrows in Fig. 8a). In (b) we show time series of horizontal components at the two stations BTO1 and JUNT. These stations suffer from data gaps lasting for 2 or more years. (For interpretation of the references to colour in this figure legend, the reader is referred to the web version of this article.)

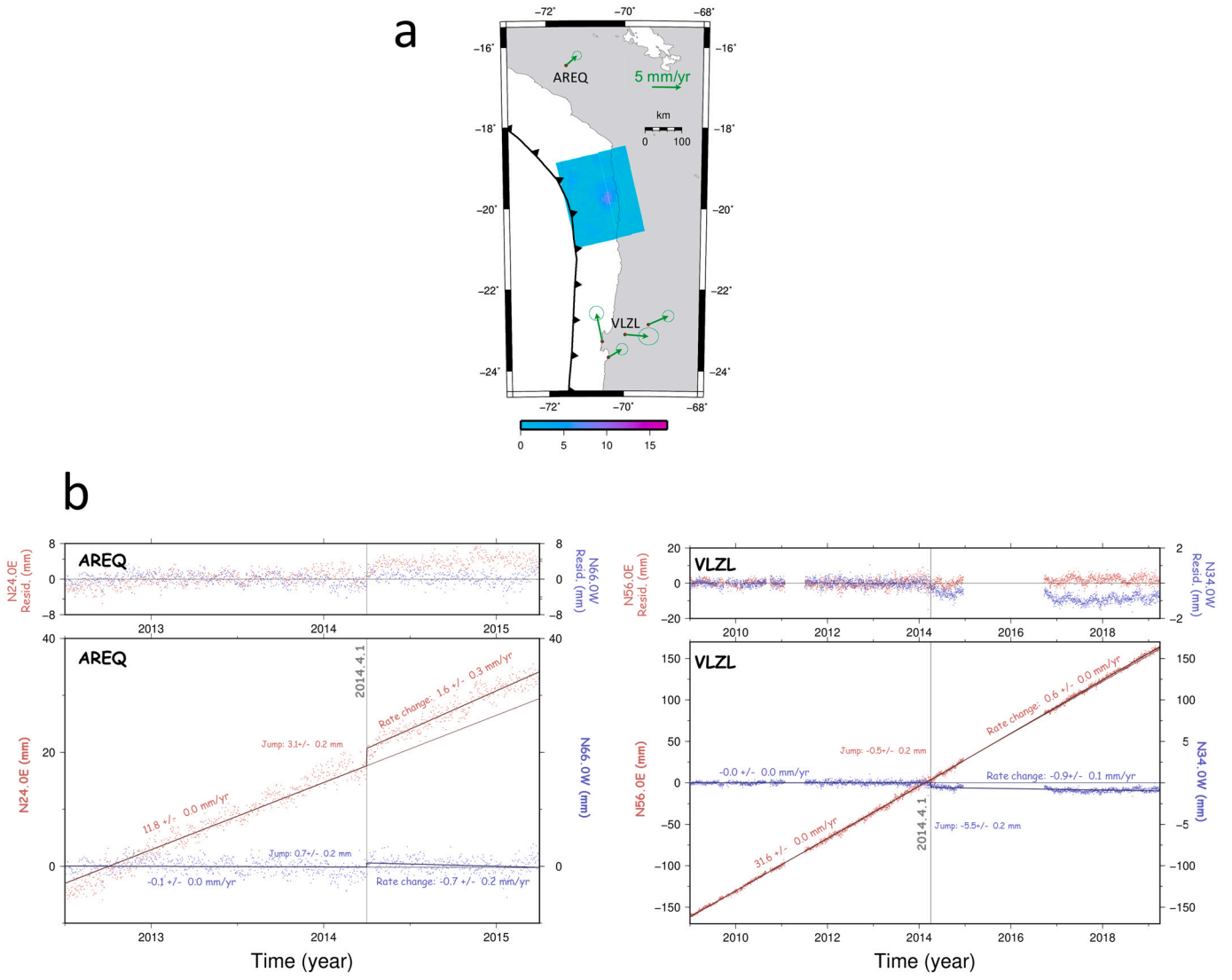

Fig. A6. (a) Horizontal velocity changes by the2014 Iquique earthquake (same as stations with green arrows in Fig. 9a). In (b) we show time series of the two stations AREQ and VLZL. (For interpretation of the references to colour in this figure legend, the reader is referred to the web version of this article.)

A.4. Time series before the 2003 Tokachi-oki earthquake

In order to confirm the influence of the postseismic movement of the 1994 Sanriku-oki earthquake on the coseismic velocity changes of the 2003 Tokachi-oki earthquake at stations in NE Honshu, we plot the baseline length (distance) between the 0027 station (Fig. 7) on the Pacific coast and the 0184 station on the Japan Sea coast. The time series are modeled with lines with breaks at 1997.0, 1998.0, 1999.0, 2000.5, 2002.0 in Fig. A7. In 1996–1998, the distance does not show significant changes due to the balance of the landward (interseismic strain) and oceanward (postseismic movement of the 1994 event). As the latter decay, the slope becomes stationary. In Fig. 7, we excluded data before 1998.0 to avoid the leakage of the influence of the 1994 earthquake into the estimation of the coseismic velocity change in 2003 September.

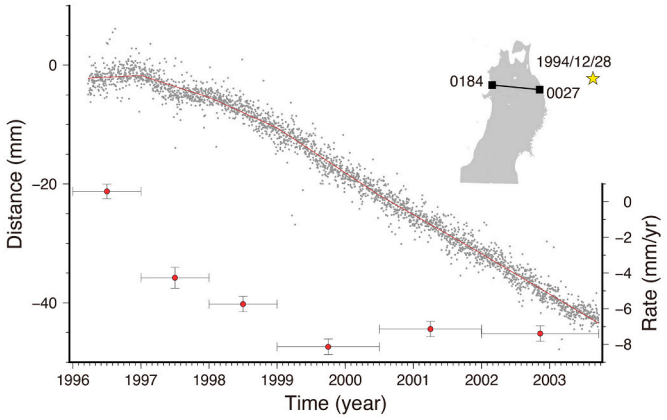

Fig. A7. The change of the baseline length connecting the 0027 and 0184 stations between the 1994 Sanriku-oki and 2003 Tokachi-oki earthquakes (the F3 solution not available before 1996 March). Slopes are estimated in different time windows of 1–1.5 years. The vertical error bars indicate 2σ uncertainties. This demonstrates that significant influence of the postseismic crustal movement extends only until ~1998.

A.5. Change in seismicity

To compare seismicity changes by large earthquakes, we removed clustered earthquakes such as swarms and aftershocks from the ISC catalog using a stochastic declustering method developed by Zhuang et al. (2004). Table A1 shows parameters estimated from fitting the ETAS models to the ISC catalog. Figs. A8 and A9 compare the seismicity before and after the application of such declustering. See Section 5.2 for the detailed discussion.

Table A1
List of parameters estimated from fitting the ETAS models to the ISC catalog.

No	Area	Earthquake	μ, events/day	A, events/day	C, day	α, M^{-1}	p	γ
1	41.5°-45 N, 143°-149°E	The 2011 Tohoku-oki	0.97	0.14	0.02	1.77	1.07	0.85
2	33°-27°S, 74°-70°W	The 2010 Maule	0.96	0.50	0.02	1.31	1.11	0.70

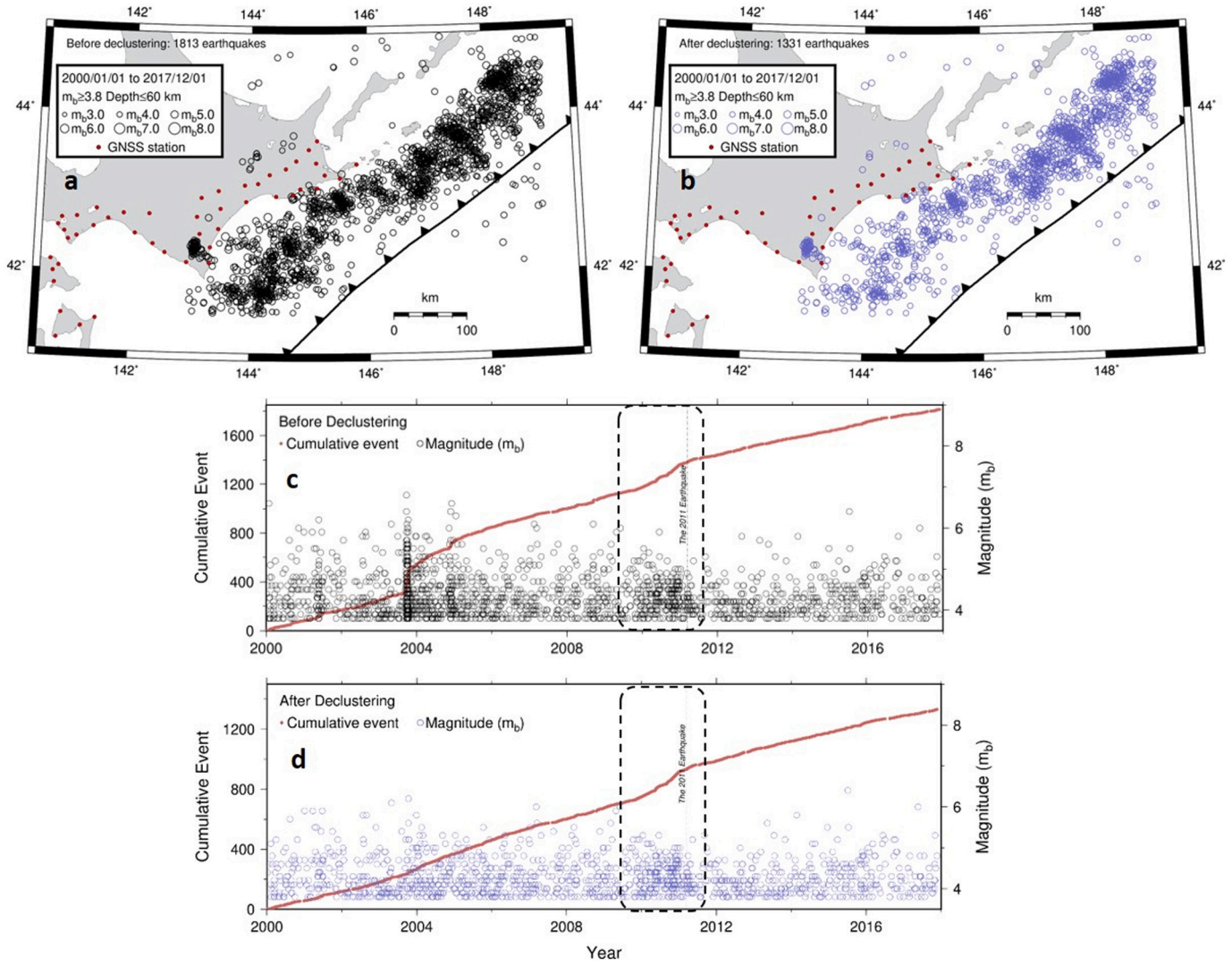

Fig. A8. Seismicity in the east coast Hokkaido before (a, c) and after (b, d) the application of declustering based on the ETAS model. There are 1813 and 1331 events before and after declustering, respectively. The dashed area indicates the period of the increase of background seismicity due to unknown mechanisms.

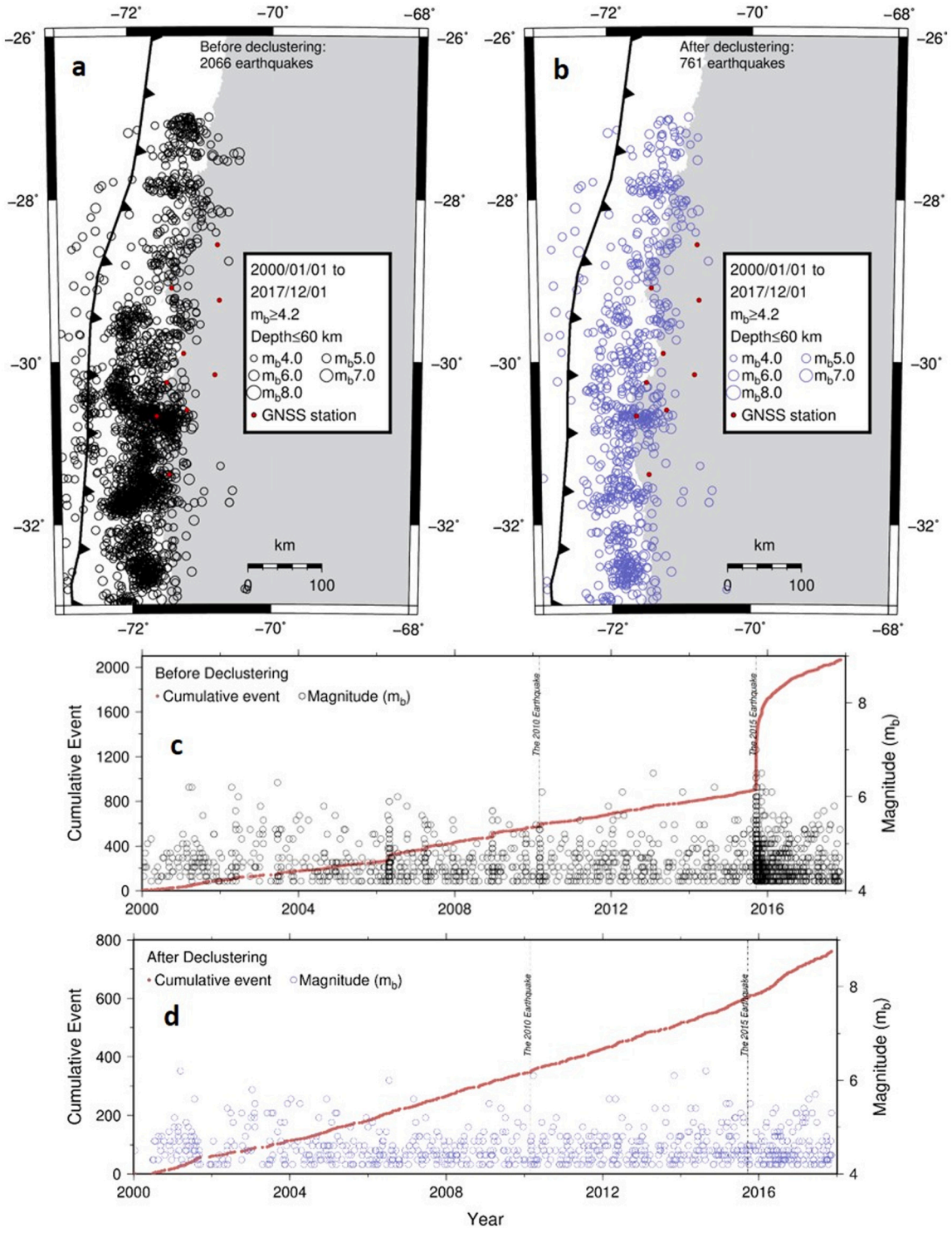

Fig. A9. Seismicity in the Pacific coast region of central Chile before (a, c) and after (b, d) the application of declustering based on the ETAS model. There are 2066 and 761 events before and after the declustering, respectively.

References

Abercrombie, R.E., Antolik, M., Ekström, G., 2003. The June 2000 M_w7.9 earthquakes south of Sumatra: Deformation in the India-Australia Plate. J. Geophys. Res. 108 (B1), 2018. https://doi.org/10.1029/2001JB000674.

Anderson, D.L., 1975. Accelerated plate tectonics. Science 187, 1077–1079.

Ardika, M., Meilano, I., Gunawan, E., 2015. Postseismic deformation parameters of the 2010 M7.8 Mentawai, Indonesia, earthquake inferred from continuous GPS observations. Asian J. Earth Sci. 8 (4), 127–133. https://doi.org/10.3923/ajes.2015.127.133.

Argus, D.F., Gordon, R.G., DeMets, C., 2011. Geologically current motion of 56 plates relative to the no-net-rotation reference frame. Geochem. Geophys. Geosyst. 12, Q11001 https://doi.org/10.1029/2011GC003751.

Blewitt, G., Hammond, W.C., Kreemer, C., 2018. Harnessing the GPS data explosion for interdisciplinary science. EOS 99. https://doi.org/10.1029/2018EO104623.

Courboulex, F., Singh, S.K., Pacheco, J.F., Ammon, C.J., 1997. The 1995 Colima-Jalisco, Mexico, earthquake (Mw 8): a study of rupture process. Geophys. Res. Lett. 24 (9), 1019–1022. https://doi.org/10.1029/97GL00945.

D'Acquisto, M., Herman, M.W., Govers, R., 2020. On the cause of enhanced landward motion of the overriding plate after a major subduction earthquake. paper presented at the American Geophysical Union Fall Meeting. Dec. 16, 2020.
Deal, M.M., Nolet, G., 1999. Slab temperature and thickness from seismic tomography 2. Izu-Bonin, Japan, and Kuril subduction zones. J. Geophys. Res. 104 (12), 28803–28812.
Feng, L., Hill, E.M., Banerjee, P., Hermawan, I., Tsang, L.L.H., Natawidjaja, D.H., Suwargadi, B.W., Sieh, K., 2015. A unified GPS-based earthquake catalog for the Sumatran plate boundary between 2002 and 2013. J. Geophys. Res. Solid Earth 120, 3566–3598. https://doi.org/10.1002/2014JB011661.
Fukahata, Y., Matsu'ura, M., 2005. General expressions for internal deformation fields due to a dislocation source in a multilayered elastic half-space. Geophys. J. Int. 161, 507–521. https://doi.org/10.1111/j.1365-246X.2005.02594.x.
Fukahata, Y., Matsu'ura, M., 2006. Quasi-static internal deformation due to a dislocation source in a multilayered elastic/viscoelastic half-space and an equivalence theorem. Geophys. J. Int. 166, 418–434. https://doi.org/10.1111/j.1365-246X.2006.02921.x.
Habermann, R.E., 1991. Seismicity rate variations and systematic changes in magnitudes in teleseismic catalogs. Tectonophysics 193 (4), 277–289. https://doi.org/10.1016/0040-1951(91)90337-R.
Hafkenscheid, E., Buiter, S.J.H., Wortel, M.J.R., Spakman, W., Bijwaard, H., 2001. Modelling the seismic velocity structure beneath Indonesia: a comparison with tomography. Tectonophysics 333, 35–46.
Hanifa, N.R., Sagiya, T., Kimata, F., Efendi, J., Abidin, H.Z., Meilano, I., 2014. Interplate coupling model off the southwestern coast of Java, Indonesia, based on continuous GPS data in 2008-2010. Earth Planet. Sci. Lett. 401, 159–171. https://doi.org/10.1016/j.epsl.2014.06.010.
Haridhi, H.A., Huang, B.S., Wen, K.L., Denzema, D., Prasetyo, R.A., Lee, C.S., 2018. A study of large earthquake sequences in the Sumatra subduction zone and its possible implications. Terr. Atmos. Ocean. Sci. 29, 635–652. https://doi.org/10.3319/TAO.2018.08.22.01.
Heki, K., Mitsui, Y., 2013. Accelerated pacific plate subduction following interplate thrust earthquakes at the Japan trench. Earth Planet. Sci. Lett. 363, 44–49. https://doi.org/10.1016/j.epsl.2012.12.031.
Heki, K., Miyazaki, S., Tsuji, H., 1997. Silent fault slip following an interplate thrust earthquake at the Japan Trench. Nature 386, 595–597.
Herring, T. A., King, R. W., Floyd, M. A., McClusky S. C., 2018. Introduction to GAMIT/GLOBK, Release 10.7. geoweb.mit.edu/gg/intro_GG.pdf.
Hoffmann, F., Metzger, S., Moreno, M., Deng, Z., Sippl, C., Ortega-Culaciati, F., Oncken, O., 2018. Characterizing afterslip and ground displacement rate increase following the 2014 Iquique Pisagua M_w 8.1 earthquake, Northern Chile. J. Geophys. Res. Solid Earth 123, 4171–4192. https://doi.org/10.1002/2017JB014970.
Husker, A., Davis, P.M., 2009. Tomography and thermal state of the Cocos plate subduction beneath Mexico City. J. Geophys. Res. 114, B04306 https://doi.org/10.1029/2008JB006039.
Ide, S., 2013. The proportionality between relative plate velocity and seismicity in subduction zones. Nat. Geosci. 6, 780–784. https://doi.org/10.1038/NGEO1901.
Iinuma, T., et al., 2012. Coseismic slip distribution of the 2011 off the Pacific Coast of Tohoku earthquake (M9.0) refined by means of seafloor geodetic data. J. Geophys. Res. Solid Earth 117. https://doi.org/10.1029/2012JB009186. B07409.
Itoh, Y., Nishimura, T., 2016. Characteristics of postseismic deformation following the 2003 Tokachi-oki earthquake and estimation of the viscoelastic structure in Hokkaido, northern Japan. Earth Planets Space 68, 156. https://doi.org/10.1186/s40623-016-0533-y.
Kanamori, H., 1978. Quantification of earthquakes. Nature 271, 411–414.
Kanamori, H., Jennings, P.C., Singh, S.K., Astiz, L., 1993. Estimation of strong ground motion in Mexico City expected for large earthquakes in the Guerrero Seismic Gap. Bull. Seismol. Soc. Am. 83 (3), 811–829.
Kelleher, J.A., 1972. Rupture zones of large South American earthquakes and some predictions. J. Geophys. Res. 77 (11), 2087–2103.
King, G.C.P., Stein, R.S., Lin, J., 1994. Static stress changes and the triggering of earthquakes. Bull. Seismol. Soc. Am. 84, 935–953.
Klein, E., Fleitout, L., Vigny, C., Garaud, J.D., 2016. Afterslip and viscoelastic relaxation model inferred from the large-scale post-seismic deformation following the 2010 M_w 8.8 Maule earthquake (Chile). Geophys. J. Int. 205, 1455–1472. https://doi.org/10.1093/gji/ggw086.
Li, S., Moreno, M., Bedford, J., Rosenau, M., Oncken, O., 2015. Revisiting viscoelastic effects on interseismic deformation and locking degree: a case study of the Peru-North Chile subduction zone. J. Geophys. Res. 120, 4522–4538. https://doi.org/10.1002/2015JB011903.
Lombardi, A.M., Cocco, M., Marzocchi, W., 2010. On the increase of background seismicity rate during the 1997-1998 Umbria-Marche, Central Italy, sequence: Apparent variation or fluid-driven triggering? Bull. Seismol. Soc. Am. 100 (3), 1138–1152. https://doi.org/10.1785/0120090077.
Loveless, J.P., 2017. Super-interseismic periods: Redifining earthquake recurrence. Geophys. Res. Lett. 44, 1329–1332. https://doi.org/10.1002/2017GL072525.
Lubis, A.M., Hashima, A., Sato, T., 2013. Analysis of afterslip distribution following the 2007 September 12 southern Sumatra earthquake using poroelastic and viscoelastic media. Geophys. J. Int. 192, 18–37. https://doi.org/10.1093/gji/ggs020.
Luo, H., Ambrosius, B., Russo, R.M., Mocanu, V., Wang, K., Bevis, M., Fernandes, R., 2020. A recent increase in megathrust locking in the southernmost rupture area of the giant 1960 Chile earthquake. Earth Planet. Sci. Lett. 537, 116200. https://doi.org/10.1016/j.epsl.2020.116200.
Materna, K., Bartlow, N., Wech, A., Williams, C., Burgmann, R., 2019. Dynamically triggered changes of plate interface coupling in Southern Cascadia. Geophys. Res. Lett. 46, 12890–12899. https://doi.org/10.1029/2019GL084395.
Mavrommatis, A., Segall, P., Johnson, K.M., 2014. A decadal-scale deformation transient prior to the 2011 Mw 9.0 Tohoku-oki earthquake. Geophys. Res. Lett. 41, 4486–4494. https://doi.org/10.1002/2014GL060139.
Melnick, D., Moreno, M., Quinteros, J., Baez, J.C., Deng, Z., Li, S., Oncken, O., 2017. The super-interseismic phase of the megathrust earthquake cycle in Chile. Geophys. Res. Lett. 44, 784–791. https://doi.org/10.1002/2016GL071845.
Métois, M., Socquet, A., Vigny, C., Carrizo, D., Peyrat, S., Delorme, A., Maureira, E., Valderas-Bermejo, M.-C., Ortega, I., 2013. Revisiting the North Chile seismic gap segmentation using GPS-derived interseismic coupling. Geophys. J. Int. 194, 1283–1294. https://doi.org/10.1093/gji/ggt183.
Mignan, A., King, G., Bowman, D., Lacassin, R., Dmowska, R., 2006. Seismic activity in the Sumatra-Java region prior to the December 26, 2004. (M_w=9.0-9.3) and March 28, 2005 (M_w=8.7) earthquake. Earth Planet. Sci. Lett. 244, 639–654. https://doi.org/10.1016/j.epsl.2006.01.058.
Miyazaki, S., Segall, P., Fukuda, J., Kato, T., 2004. Space time distribution of afterslip following the 2003 Tokachi-oki earthquake: Implications for variations in fault zone frictional properties. Geophys. Res. Lett. 31, L06623 https://doi.org/10.1029/2003GL019410.
Moreno, M., et al., 2012. Toward understanding tectonic control on the M_w 8.8 2010 Maule Chile earthquake. Earth Planet. Sci. Lett. 321-322, 152–165. https://doi.org/10.1016/j.epsl.2012.01.006.
Nakagawa, H., Toyofuku, T., Kotani, K., Miyahara, B., Iwashita, C., Kawamoto, S., Hatanaka, Y., Munekane, H., Ishimoto, M., Yutsudo, T., Ishikura, N., Sugawara, Y., 2009. Development and validation of GEONET new analysis strategy (Version 4). J. Geogr. Surv. Inst. 118, 1–8 (in Japanese).
Natawidjaja, D.H., Sieh, K., Chlieh, M., Galetzka, J., Suwargadi, B.W., Cheng, H., Edwards, R.L., Avouac, J.-P., Ward, S.N., 2006. Source parameters of the great Sumatran megathrust earthquakes of 1797 and 1833 inferred from coral microatolls. J. Geophys. Res. 111, B06403 https://doi.org/10.1029/2005JB004025.
Ozawa, S., Kaidzu, M., Murakami, M., Imakiire, T., Hanataka, Y., 2004. Coseismic and postseismic crustal deformation after the M_w 8 Tokachi-oki earthquake in Japan. Earth Planet Space 56, 675–680.
Perfettini, H., Avouac, J.-P., Ruegg, J.C., 2005. Geodetic displacements and aftershocks following the 2001 M_w=8.4 Peru earthquake: Implications for the mechanics of the earthquake cycle along subduction zones. J. Geophys. Res. 110 https://doi.org/10.1029/2004JB003522. B09404.
Pritchard, M.E., Simons, M., Rosen, P.A., Hensley, S., Webb, F.H., 2002. Co-seismic slip from the 1995 July 30 Mw = 8.1 Antofagasta, Chile, earthquake as constrained by InSAR and GPS observations. Geophys. J. Int. 150, 362–376. https://doi.org/10.1046/j.1365-246X.2002.01661.x.
Ruiz, S., Moreno, M., Melnick, D., del Campo, F., Poli, P., Baez, J.C., Leyton, F., Madariaga, R., 2017. Reawakening of large earthquakes in south Central Chile: the 2016 M_w 7.6 Chiloé event. Geophys. Res. Lett. 44, 6633–6640. https://doi.org/10.1002/2017GL074133.
Satake, K., Nishimura, Y., Putra, S.P., Gusman, A.R., Sunendar, H., Fujii, Y., Tanioka, Y., Latief, H., Yulianto, E., 2012. Tsunami source of the 2010 Mentawai, Indonesia earthquake inferred from tsunami field survey and waveform modeling. Pure Appl. Geophys. 170, 1567–1582. https://doi.org/10.1007/s00024-012-0536-y.
Schurr, B., Asch, G., Rosenau, M., Wang, R., Oncken, O., Barrientos, S., Salazar, P., Vilotte, J.P., 2012. The 2007 M7.7 Tocopilla northern Chile earthquake sequence: Implications for along-strike and downdip rupture segmentation and megathrust frictional behavior. J. Geophys. Res. 117 https://doi.org/10.1029/2011JB009030. B05305.
Scire, A., Zandt, G., Beck, S., Long, M., Wagner, L., 2017. The deforming Nazca slab in the mantle transition zone and lower mantle: Constraints from teleseismic tomography on the deeply subducted slab between 6°S and 32°S. Geosphere 13, 665–680. https://doi.org/10.1130/GES01436.1.
Segou, M., Parsons, M., 2018. Testing earthquake links in Mexico from 1978 to the 2017 M = 8.1 Chiapas and M = 7.1 Puebla shocks. Geophys. Res. Lett. 45, 708–714. https://doi.org/10.1002/2017GL076237.
Sun, T., Wang, K., Iinuma, T., Hino, R., He, J., Fujimoto, H., Kido., M., Osada, Y., Miura, S., Ohta, Y., Hu, Y., 2014. Prevalence of viscoelastic relaxation after the 2011 Tohoku-oki earthquake. Nature,514, 84–87. doi:https://doi.org/10.1038/nature13778.
Shao, Z., Zhan, W., Zhang, L., Xu, J., 2015. Analysis of the far field Co-seismic and Post-seismic responses caused by the 2011 M_w 9.0 Tohoku-Oki earthquake. Pure Appl. Geophys. 173, 411–424. https://doi.org/10.1007/s00024-015-1131-9.
Tajima, F., Mori, J., Kennet, B.L.N., 2013. A review of the 2011 Tohoku-oki earthquake (M_w 9.0): Large-scale rupture across heterogeneous plate coupling. Tectonophysics 586, 15–34. https://doi.org/10.1016/j.tecto.2012.09.014.
Tanioka, Y., Katsumata, K., 2007. Tsunami generated by the 2004 Kushiro-oki earthquake. Earth Planets Space 59, e1–e3.
Uchida, N., Asano, Y., Hasegawa, A., 2016. Acceleration of regional plate subduction beneath Kanto, Japan, after the 2011 Tohoku-oki earthquake. Geophys. Res. Lett. 43, 9002–9008. https://doi.org/10.1002/2016GL070298.
Vigny, C., et al., 2011. The 2010 M_w 8.8 Maule megathrust earthquake of Central Chile, monitored by GPS. Science 332, 1417–1421. https://doi.org/10.1126/science.1204132.
Villegas-Lanza, J.C., Chlieh, M., Cavalié, O., Tavera, H., Baby, P., Chire-Chira, J., Nocquet, J.-M., 2016. Active tectonics of Peru: Heterogeneous interseismic coupling along the Nazca megathrust, rigid motion of the Peruvian Sliver, and Subandean shortening accommodation. J. Geophys. Res. 121, 7371–7394. https://doi.org/10.1002/2016JB013080.
Wang, K., Hu, Y., He, J., 2012. Deformation cycles of subduction earthquakes in a viscoelastic Earth. Nature 484, 327–332. https://doi.org/10.1038/nature11032.

Wiemer, S., Wyss, M., 2000. Minimum magnitude of completeness in earthquake catalogs: examples from Alaska, the Western United States, and Japan. Bull. Seismol. Soc. Am. 90, 859–869. https://doi.org/10.1785/0119990114.

Yamagiwa, S., Miyazaki, S., Hirahara, K., Fukahata, Y., 2015. Afterslip and viscoelastic relaxation following the 2011 Tohoku-oki earthquake (M_w9.0) inferred from inland GPS and seafloor GPS Acoustic data. Geophys. Res. Lett. 42, 66–73. https://doi.org/10.1002/2014GL061735.

Zhuang, J.O., Ogata, Y., Vere-Jones, D., 2004. Analyzing earthquake clustering features by using stochastic reconstruction. J. Geophys. Res. 109, B05301 https://doi.org/10.1029/2003JB002879.